© 2022. Published by The Company of Biologists Ltd | Development (2022) 149, dev201052. doi:10.1242/dev.201052

STEM CELLS AND REGENERATION

TECHNIQUES AND RESOURCES ARTICLE

Self-organizing *in vitro* mouse neural tube organoids mimic embryonic development

JiSoo Park[1], Hao-An Hsiung[1], Irina Khven[2], Gioele La Manno[2] and Matthias P. Lutolf[1,3,4,*]

ABSTRACT

The embryonic neural tube is the origin of the entire adult nervous system, and disturbances in its development cause life-threatening birth defects. However, the study of mammalian neural tube development is limited by the lack of physiologically realistic three-dimensional (3D) *in vitro* models. Here, we report a self-organizing 3D neural tube organoid model derived from single mouse embryonic stem cells that exhibits an *in vivo*-like tissue architecture, cell type composition and anterior-posterior (AP) patterning. Moreover, maturation of the neural tube organoids showed the emergence of multipotent neural crest cells and mature neurons. Single-cell transcriptome analyses revealed the sequence of transcriptional events in the emergence of neural crest cells and neural differentiation. Thanks to the accessibility of this model, phagocytosis of migrating neural crest cells could be observed in real time for the first time in a mammalian model. We thus introduce a tractable *in vitro* model to study some of the key morphogenetic and cell type derivation events during early neural development.

KEY WORDS: Neural tube, Organoid, Neural development, Anterior-posterior patterning, Neural crest cells

INTRODUCTION

Given the developmental importance of the neural tube and the biological richness of its morphogenesis and patterning, it is somewhat surprising that its in-depth, real-time study is hampered by the availability of only relatively few models. Indeed, studies of neural tube development to date have been possible mainly through the use of animal models, which require labor-intensive, technically challenging and low-throughput interventions. Additionally, the tracking of key cellular events in real time, which is important for understanding various cellular processes, is complicated in animals. However, 3D organoids have emerged as faithful *in vitro* models that recapitulate key developmental processes to better study the emergence and function of organ development with greater experimental accessibility and reproducibility in real time (Huch et al., 2017; Rossi et al., 2018; Takebe and Wells, 2019). The development of neural tube organoids and their accessibility should help address the cellular organization and connectivity of the neural network, which previously seemed impossible.

There are many specific and tightly controlled events that must take place in a model to replicate *in vivo* neural tube development. In the developing mammalian embryo, the neural tube emerges by the formation of a tube through an invagination of the neuroectoderm, which is derived from the embryonic epiblast after gastrulation (Sadler, 2005; Greene and Copp, 2009). The structure contains a single continuous lumen extending the entire length of the embryo, called the neural canal (Thouvenin et al., 2020), that forms the early ventricular system that is crucial for maintaining homeostasis and protecting central nervous system tissues (Fame and Lehtinen, 2020; Fame et al., 2020). The neural tube develops to specify mature, region-specific cell types along its anterior-posterior (AP) and dorsal-ventral (DV) axis in a remarkably sophisticated spatio-temporal patterning process controlled by morphogens and interactions with surrounding tissue types (Yamaguchi, 2001; Deschamps and Van Nes, 2005; Schilling, 2008; Briscoe and Small, 2015; Sagner and Briscoe, 2017, 2019). In particular, multipotent neural crest cells emerge, delaminate and migrate from the dorsal side of the neural tube and differentiate into a wide variety of cell types that contribute to the peripheral nervous system, the endocrine system and the facial skeleton, among many others (Le Douarin et al., 2004; Dupin, 2006). The abnormalities in their development can cause congenital neurocristopathies such as Treacher Collins (Vega-Lopez et al., 2018; Sato et al., 2019; Pilon, 2021). Even though several *in vitro* neural tube models have been reported recently (Meinhardt et al., 2014; Ranga et al., 2016; Zheng et al., 2019; Ogura et al., 2018; Duval et al., 2019; Veenvliet et al., 2020; Libby et al., 2021; Demers et al., 2016; Rifes et al., 2020), to date, there does not appear to be a suitable model that recapitulates the *in vivo* morphology, coordinated AP patterning and emergence of the neural crest.

We present here a self-organizing neural tube organoid that mimics the mouse embryonic neural tube in terms of its morphology, cell type composition and aspects of patterning. When exposed to a sequence of epiblast culture conditions and neural differentiation conditions in 3D Matrigel, single mouse embryonic stem cells (mESCs) develop into spontaneously elongating neuroepithelial tissues organized with key hallmarks of the neural tube. Single cell transcriptomics revealed the presence of regionalized cell types spanning the region from the midbrain to the spinal cord along the AP axis of the embryo. In long-term culture experiments for organoid maturation, we observed the emergence of multipotent neural crest cells and mature neurons. Tracking this development by single-cell transcriptomic analysis at serial time points revealed the transcriptomic details of neural crest cell

[1]Laboratory of Stem Cell Bioengineering, Institute of Bioengineering, School of Life Sciences and School of Engineering, École Polytechnique Fédérale de Lausanne (EPFL), Lausanne 1015, Vaud, Switzerland. [2]Laboratory of Neurodevelopmental Systems Biology, Brain Mind Institute, School of Life Sciences, École Polytechnique Fédérale de Lausanne (EPFL), Lausanne 1015, Vaud, Switzerland. [3]Institute of Chemical Sciences and Engineering, School of Basic Science, École Polytechnique Fédérale de Lausanne (EPFL), Lausanne 1015, Vaud, Switzerland. [4]Roche Institute for Translational Bioengineering (ITB), Roche Pharma Research and Early Development, Roche Innovation Center Basel, Basel 4058, Switzerland.

*Author for correspondence (matthias.lutolf@epfl.ch)

M.P.L., 0000-0002-5898-305X

Handling Editor: James Briscoe
Received 22 June 2022; Accepted 25 August 2022

Development (2022) 149, dev201052. doi:10.1242/dev.201052

formation and neural differentiation. Collectively, the accessibility and scalability of these organoids make them a potent model of the developing neural tube, allowing the study of key mechanisms involved in self-organization, cell fate specification and neural crest cell development *in vivo*.

RESULTS

Generation of self-elongating neural tube organoid

To recapitulate neural tube development *in vivo*, we postulated the generation of a self-organizing neural tube organoid derived from the epiblast. To generate such structures, we first embedded a suspension of single mESCs in Matrigel and promoted their differentiation towards epiblast fates and neural lineages, sequentially. Specifically, to physiologically mimic the neuroepithelium development *in vivo*, the cells were cultured for the first 3 days in serum-free N2B27 medium containing bFGF and activin A (Brons et al., 2007; Hayashi et al., 2011) to guide them toward an epiblast state. The cells were then cultured in N2B27 to induce neural differentiation (Fig. 1A). We observed that mESCs form cysts and spontaneously elongate into structures harboring a continuous lumen and displaying characteristic features of the embryonic neural tube (Fig. 1B, Fig. S1, Movie 1). Time-lapse imaging between day (D) 4 and D6 using a live cell actin probe to capture the lumen of apicobasally polarized organoids demonstrated that the neuroepithelial cysts indeed elongate and such elongation was concomitant with that of their lumen (Fig. S1B, Movie 1). Time-course images from D0 to D6 confirmed that self-elongating organoids emerged from a single cell (Movie 1). Elongation efficiency was 52.0±4.5% (n=9 Matrigel drops, N=3 replicates) (Fig. S1C) and the length and elongation index increased about threefold between D4 and D6 (Fig. S1D). Neural tube organoid formation was reproducible in three different mESC lines that were tested, each line requiring an optimal cell seeding density (Fig. S2, Table S1).

Neural tube organoid harbors the key hallmarks of developing neural tube *in vivo*

To assess the similarity of the organoids to the embryonic neural tube, we examined the expression of key markers of neural tube development *in vivo*. This revealed progressive differentiation from a pluripotent state toward neuroprogenitor identities. Specifically, quantitative PCR analysis of organoids between D3 and D6 shows a gradual transition from epiblast to neuroprogenitor fate, with epiblast markers *Pou5f1* (also known as *Oct4*), *Otx2* and *Fgf5* gradually decreasing over time, and neuroprogenitor markers *Sox1*, *Sox2* and *Pax6* gradually increasing as the organoids develop (Fig. 1C).

In addition to neuroprogenitor markers, our organoids also exhibit key hallmarks of the tissue architecture of the embryonic neural tube. For example, they also possess apicobasal polarity, as demonstrated by the apical localization of the tight junction marker ZO-1 and the presence of apical domain markers prominin 1 and PKCζ (Fig. 1D). Immunofluorescence staining confirmed the presence of neuroprogenitor cells expressing the markers SOX1, SOX2, PAX6 and nestin (Fig. 1E). In addition, confocal imaging revealed the presence of primary cilia (marked by ARL13B) at the apical membrane of the organoids (Fig. 1F, Movie 2), which are essential for the sonic hedgehog (Shh) pathway and the planar cell polarity (PCP) pathway during neural tube development *in vivo* (Bay and Caspary, 2012). Moreover, light-sheet microscopy showed a highly organized 3D structure of the neuroepithelium bounding the elongated lumen, which confirms that this is indeed continuous throughout the organoid (Fig. 1G, Movie 3). This elongated tubular lumen resembles the neural canal of a developing neural tube, which forms the early ventricular system that is essential for tissue

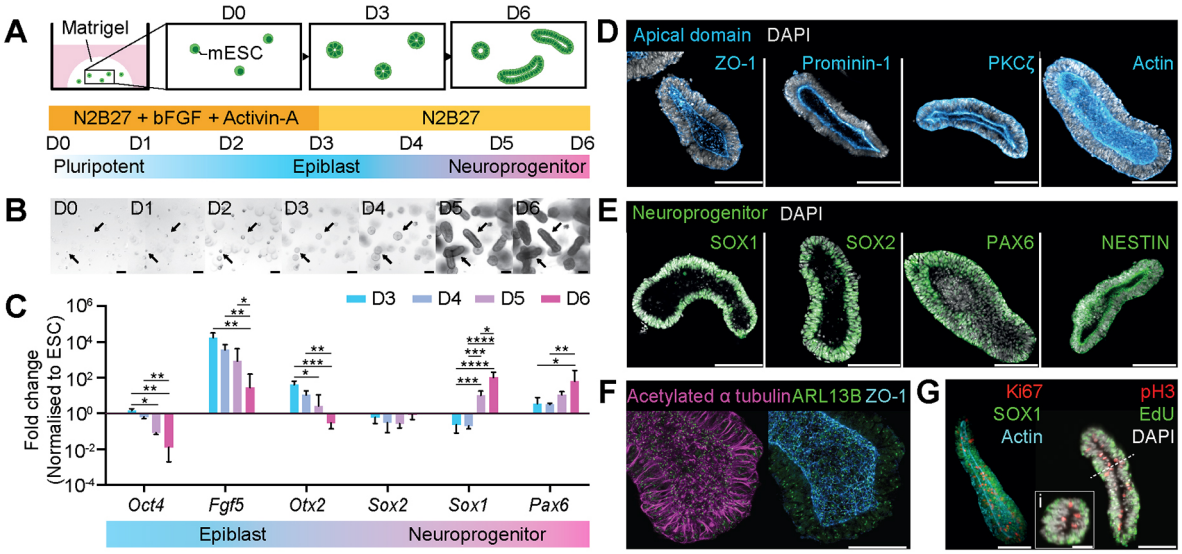

Fig. 1. Self-elongating neural tube organoids harboring the hallmarks of the native neural tube. (A) Schematic of a self-elongating neural tube organoid culture in 3D along with the differentiation protocol (details in the Materials and Methods). Single mESCs were embedded in Matrigel and their differentiation promoted towards epiblast fates and neural lineages, sequentially. (B) Representative bright-field time course images of the organoids cultured from D0 to D6. Arrows indicate the progress of single mESCs developing into self-organizing neural tube organoids. (C) Time course of early developmental marker expression, as analyzed by qPCR between D3 and D6. The measured epiblast markers were *Oct4*, *Fgf5* and *Otx2*, and the neuroprogenitor markers were *Sox2*, *Sox1* and *Pax6*. (D) The neural tube organoids are apicobasally polarized with a single elongated lumen that is stained for the tight junction marker ZO-1, the apical domain marker prominin 1 and PKCζ restricted at the apical domain. (E) The neural tube organoids express neuroprogenitor markers such as SOX1, SOX2, PAX6 and nestin. (F) Confocal microscopy revealed the presence of primary cilia (ARL13B) in the apical membrane surface of neural tube, as *in vivo*. (G) Light-sheet imaging confirms the presence of a single elongated lumen in the organoids by actin staining surrounded by SOX1$^+$ neuroepithelial cells, with apically localized mitotic cells (Ki67$^+$ cells and pH3$^+$ cells) and basally located S-phase cells (EdU$^+$ cells) indicating interkinetic nuclear migration, one of the key hallmarks of *in vivo* neuroepithelia. Scale bars: 100 µm in D,E,G; 50 µm in F,Gi.

Development (2022) 149, dev201052. doi:10.1242/dev.201052

homeostasis of the nervous system. Furthermore, the basal localization of EdU-labeled DNA synthesis phase (S phase) cells and the apical localization of $pH3^+$ mitotic cells (M phase) are indicative of characteristic division patterns of interkinetic nuclear migration, a defining feature of cell behavior in the embryonic pseudostratified neuroepithelium (Baye and Link, 2007; Miyata et al., 2015) (Fig. 1G, Fig. S3, Movie 4). Quantification of the distance of M-phase cells ($pH3^+$) and S-phase cells (EdU^+) from the apical domain (prominin 1^+) showed the apical localization of $pH3^+$ mitotic cells (Fig. S3A). Time-lapse imaging captured and confirmed the interkinetic nuclear migration movement of the cells in the neural tube organoids (Fig. S3B, Movie 4). Altogether, these results suggest that the neural tube organoids both physiologically and morphologically recapitulate key features of developing neural tube *in vivo*.

Neural tube organoid comprises diverse cell types along the AP axis

To better characterize the cellular diversity of organoids, we performed single cell RNA sequencing (scRNAseq) of cells isolated from D6 organoids (n=4478 cells, N=2 replicates). A clustering analysis using a shared nearest neighbor modularity algorithm followed by an analysis of the markers characterizing each cluster identified a total of six cell types (Fig. 2A,B). The organoid is predominantly composed of neuroprogenitor cells from different AP axis regions of the neural tube, which include the midbrain (*En1*$^+$ and *En2*$^+$), hindbrain (*Crabp1*$^+$ and *Egr2*$^+$) and spinal cord (*Pax6*$^+$ and *Hoxb9*$^+$). The remainder of the cells consists of the caudal epiblast (*Pou5f1*$^+$, *Cdx2*$^+$ and *Wnt8a*$^+$), surface ectoderm (*Krt8*$^+$ and *Krt18*$^+$) and mesenchyme (*Twist1*$^+$ and *Snai1*$^+$) (Table S7).

To verify the spatial organization of AP axial identity cell types in a single organoid, we performed single-molecule fluorescence *in situ* hybridization (smFISH). We examined two pairs of genes: *Otx2* (midbrain) and *Gbx2* (hindbrain); and *Hoxb1* (hindbrain) and *Hoxb9* (spinal cord) (Fig. 2C). Co-expression levels of *Otx2* and *Gbx2* projected on UMAP showed that these two genes are expressed in a mutual exclusive manner (Fig. 2D). smFISH revealed their spatial organization along the AP axis of the organoid (Fig. 2E; *Otx2* in green and *Gbx2* in magenta). On the other hand, a higher level of *Hoxb1* and *Hoxb9* co-expression was observed, which was confirmed by their spatial arrangement visualized using smFISH (Fig. 2G). *Hoxb1* signal spots were detected throughout the organoid, whereas *Hoxb9* signal spots were localized at one end of the organoid, indicating the posterior part of the organoid. The expression of a broad spectrum of Hox genes along the AP axis in the organoid analyzed by scRNAseq and qPCR supports these results (Fig. 2F, Fig. S4). Indeed, as shown in Fig. S4A, anterior Hox genes were expressed in the majority of cells that made up the organoids, whereas posterior Hox genes were expressed in more limited cell populations. Crucially, the range of Hox gene expression in the organoids extended from *Hox1* to *Hox9*, corresponding to regions of the embryonic neural tube ranging from the cervical to the beginning of lumbar levels. The same range of Hox gene expression was confirmed by qPCR analysis (Fig. S4B). From these results, we conclude that the genes for AP axis identity are spatially organized in a single organoid. Importantly, we were able to obtain such patterning without the need for 'artificial' posterization, e.g. by using CHIR99021 or retinoic acid (RA), as in previous studies (Meinhardt et al., 2014; Ranga et al., 2016; Turner et al., 2017; Beccari et al., 2018; Veenvliet et al., 2020). Immunofluorescence imaging over time against the neuromesodermal progenitor (NMP) markers SOX2 and T/brachyury from D3 to D6, and the results of scRNAseq analysis also confirmed that there was no NMP in the organoid (Fig. S5). These results indicate that the axial elongation of the neural tube organoid is not driven by NMPs, as is the case with other axially elongated *in vitro* tissue models, such as gastruloids (Turner et al., 2017; Beccari et al., 2018; Veenvliet et al., 2020).

To understand the difference in cell type composition between the organoids that are elongated (D6 organoids) and not elongated (D6 NE organoids), we performed scRNAseq of these two organoid types (cultured under the same conditions) at day 6 (Fig. S6). One cell type that was preferentially present in D6 organoids compared with the D6 NE organoids was the spinal cord (24.4% of the D6 and 8% of the D6 NE organoids, respectively) (Fig. S6A). Visualization of Hox gene expression in these two groups reveals that the D6 organoids have relatively stronger expression of posterior Hox genes, whereas the D6 NE organoids express anterior genes more strongly (Fig. S6B). These data suggest that there may be a relationship between axial elongation and Hox gene expression that could explain the elongation of D6 organoids rather than D6 NE organoids. However, further studies on the mechanisms involved are needed to clarify the relationship between elongation and the development of spinal cord cell identities.

Neural crest cells and neurons emerge from mature neural tube organoids

As the neural tube develops and expands, there are two major developmental events. First, neural crest cells emerge from the dorsal side of the neural tube, which then migrate out and contribute to the development of various tissues from the peripheral nervous system to the facial skeleton. Second, neuroprogenitors of the neural tube differentiate into more mature neurons, such as motor neurons and interneurons. As our neural tube organoids exhibit some of the hallmarks of the native neural tube, we hypothesized that they would also retain the capacity to generate neural crest cells and mature neurons *in vitro*. To test this, we harvested and re-embedded in a Matrigel drop a single organoid and tested whether it could further mature from D6 onwards (Fig. 3A). Time-lapse imaging of re-embedded organoids from D6 to D8 revealed two main types of maturation events: neural crest cells and neurons (Fig. 3B, Movie 5). By quantifying the proportion of emergence of these two cell types from D7 to D10, we observed that neural crest cell emergence happened earlier than neurite outgrowth (Fig. 3C). From D9 onward, the majority of organoids had both neural crest cells and neurons. These two modes of organoid maturation were further characterized.

First, the process of the outward emergence and migration of neural crest cells in 3D from the organoids was captured by the time-lapse imaging (Fig. 3B, left box, Movie 5). Its adequate accessibility allowed us to observe the delamination, migration, cell division and phagocytosis of neural crest cells (Fig. S7, Movie 6). Especially, it was intriguing to observe the phagocytosis event of neural crest cells, which has not been reported in mammals, only in zebrafish, due to its limited accessibility (Zhu et al., 2019) (Fig. S7C, Movie 6). This clearly suggests that our model could provide a new approach for answering questions in the field. Those migratory cells were later confirmed to be neural crest cells expressing neural crest cell markers such as AP2α, nestin and SOX10 by immunofluorescence on D8 (Fig. 3D, Movie 7). Furthermore, culture of the neural crest cells for 1 month revealed the multipotency of the neural crest cells (Fig. S8). The derivation of mature neurons (βIII tubulin$^+$), peripheral nervous system neurons

Development (2022) 149, dev201052. doi:10.1242/dev.201052

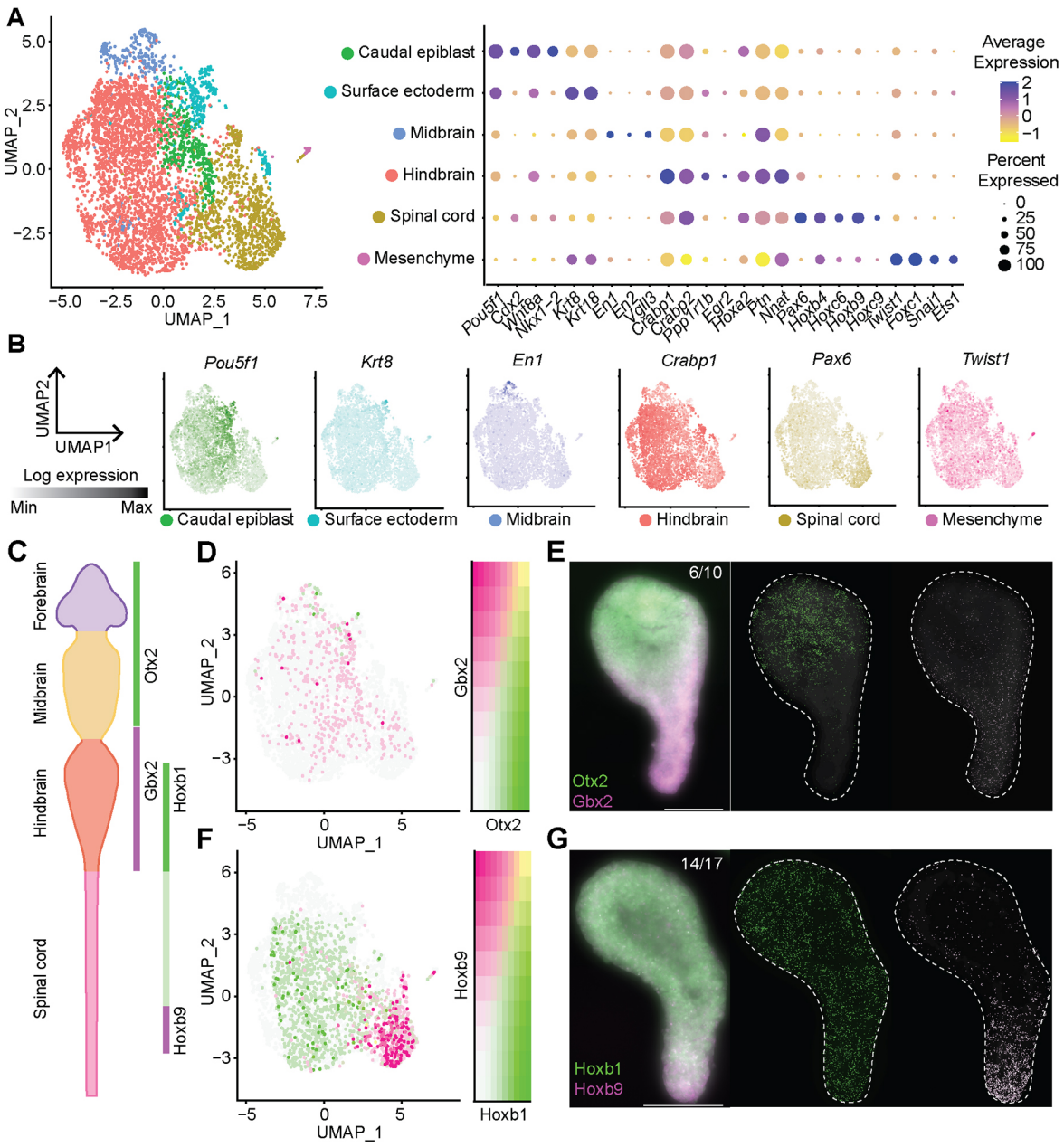

Fig. 2. Single-cell transcriptomics of the self-elongating neural tube organoids reveals the specified cell types along anterior-posterior axis of the neural tube. (A) Single-cell RNA-sequence clusters on a UMAP projection of a self-elongating neural tube organoid at D6 revealed six cell types: caudal epiblast, surface ectoderm, midbrain, hindbrain, spinal cord and mesenchyme (n=4478 cells, N=2 replicates). The key markers of each cell type are presented as a dot plot showing their average expression level and the percentage of expression in each cell type cluster: *Pou5f1* and *Cdx2* for caudal epiblast; *Krt8* and *Krt18* for surface ectoderm; *En1* and *En2* for midbrain; *Crabp1* and *Egr2* for hindbrain; *Pax6* and *Hoxb9* for spinal cord; and *Twist1* and *Foxc1* for mesenchyme. (B) The expression of the representative marker of each cell type was visualized on a UMAP projection mainly identifying the specified neural tube cell types along the anterior-posterior (AP) axis: midbrain, hindbrain and spinal cord. (C) The pairs of markers that were targeted using single-molecule fluorescence *in situ* hybridization (smFISH) to visualize the spatial patterning along the AP axis of the neural tube organoid: *Otx2* (midbrain) and *Gbx2* (hindbrain); and *Hoxb1* (hindbrain) and *Hoxb9* (spinal cord). (D,E) The co-expression level of *Otx2* and *Gbx2* was projected on UMAP and their spatial organization was verified by smFISH with *Otx2* in green and *Gbx2* in magenta. Those two genes were expressed in a mutually exclusive way in a single organoid showing the midbrain and hindbrain compartment. (F,G) The co-expression level of *Hoxb1* and *Hoxb9* was projected on UMAP and their spatial organization was verified by smFISH with *Hoxb1* in green and *Hoxb9* in magenta. *Hoxb1* was expressed overall in the organoid, whereas *Hoxb9* was expressed at one end of the organoid. Fractions in the top right corner in E and G indicate the number of spatially patterned samples/the total sample number. Scale bars: 100 µm.

(peripherin$^+$), glia (GFAP$^+$ and S100β$^+$), adipocytes (bodipy$^+$ indicating lipid droplet) and smooth muscle cells (SM22α$^+$) from neural crest cells suggests that the neural crest cells derived from organoids are multipotent, with the capacity to differentiate into not only ectodermal but also mesenchymal cell types.

The other type of maturation involved neural differentiation (Fig. 3B, right box, Movie 5). Immunofluorescence on D10 showed that these neurons were TUJ1$^+$ (neuron marker) and BRN3a$^+$ (dorsal neuron marker), indicating that the neural progenitors of the neural tube were differentiated into dorsal neurons. As shown in previous

Development (2022) 149, dev201052. doi:10.1242/dev.201052

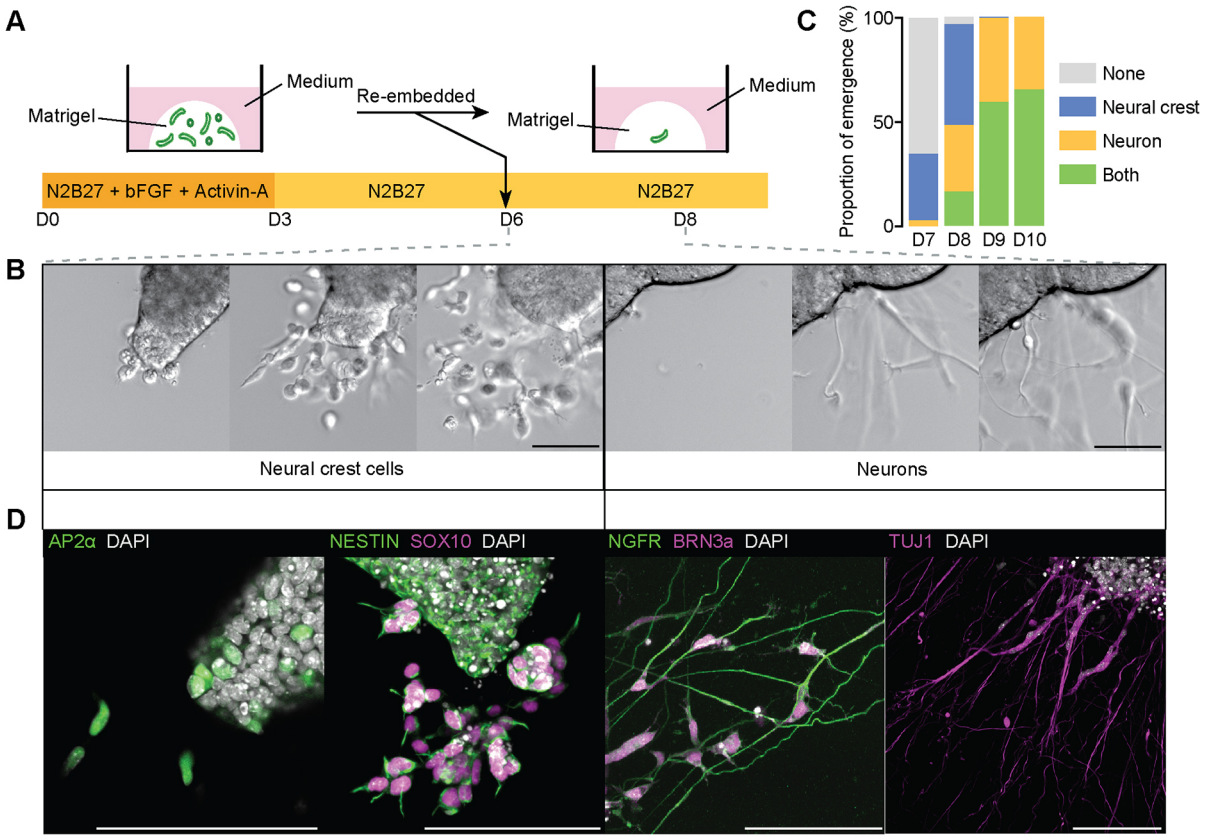

Fig. 3. Neural tube organoids mature into neural crest cells and neurons. (A) Schematic representation of long-term organoid culture from D6 onwards. The organoids were harvested and re-embedded in Matrigel on D6 and cultured further in N2B27 medium. (B) The bright-field time-lapse imaging between D6 and D8 revealed two types of organoid maturation: neural crest cells (left box) and neurons (right box). The left box shows the emergence, delamination and migration of neural crest cells from the neural tube organoid. The right box shows the neurite outgrowths that indicate the neurons in the neural tube organoid. (C) The proportions of the emergence of neural crest cell and neuron were quantified during maturation from D7 to D10 (n=112). Neural crest cells emerged earlier than the neurite outgrowth of the neurons; from D9 onwards, both neural crest cells and neurons emerged in the majority of the organoids. (D) Immunofluorescence staining of the organoids against the markers of neural crest cells and neurons confirmed their emergence. The cells that migrated from the D8 organoid expressed the neural crest cell markers AP2α, nestin and SOX10; the neurites extending from the D10 organoid expressed the neuron markers NGFR and TUJ1; the nuclei of the cells with neurites expressed the dorsal interneuron marker BRN3α. Scale bars: 100 µm.

studies, neural tissue differentiated from pluripotent stem cells without ventral morphogens has a default dorsal fate (Meinhardt et al., 2014; Ranga et al., 2016), and our organoids cultured without ventral morphogens lack the ventral cell types of the neural tube (Fig. S9), supporting BRN3a$^+$ neurons. Of note, ventralized neural tube organoids can be obtained by exposing organoids from D3 to D5 to 500 nM smoothened agonist (SAG, ventral signal) (Fig. S9A). qPCR analysis of D6 organoids for marker genes along the DV axis showed that control organoids have default dorsal identity with low expression of ventral marker genes, but ventralized organoids show upregulated ventral marker genes (Fig. S9B). Immunostaining against the ventral markers FOXA2 and OLIG2 on D6 organoids also showed that the organoids can adopt a ventral identity in response to ventral morphogens (Fig. S9C). Altogether, these data demonstrate that our organoid can be a new tool for studying the emergence, delamination and migration of neural crest cells, and the neural differentiation of the neural tube in an easily accessible and tractable fashion.

scRNAseq analysis of neural crest and neural differentiation in mature organoids

To better understand neural tube organoid maturation at the single cell level, we performed scRNAseq on D6, D7, D8 and D10 organoids, identifying the key cell types that emerge during maturation (Fig. 4A, Fig. S10, Table S8). The transition in the ratio of cell types from D6 to D10 shows a similar trend to the earlier observation that neural crest cells appear before neurons (Figs 4B, 3C). The major cell types of D6 organoid are mid/hindbrain and spinal cord cells, as shown before. Noticeably, we also identified pre-EMT (epithelial-mesenchymal transition) neural crest cell clusters (*Bmp6*$^+$ and *Msx1*$^+$) (Fig. 4A,C,D). Key to determine the regional AP identity of the pre-EMT neural crest is the expression of Hox genes, and both cranial and vagal/trunk neural crest clusters were identified (Fig. 4C, Fig. S11A). On D7, migratory neural crest cells (*Sox10*$^+$ and *Foxd3*$^+$) appear as a trajectory of pre-EMT cranial neural crest cells, and because they show low expression of Hox genes, they were identified as migratory cranial neural crest cells (Fig. 4A,C,D, Fig. S11A). Interestingly, single-cell transcriptomic analysis captured the sequence of transcriptional events during neural crest cell development. Neural crest cells delaminate by EMT between emergence and migration, and key markers of delamination (*Dlx5*$^+$ and *Pdgfra*$^+$) could be detected in cells in the pathway between the pre-EMT neural crest cells and the migrating neural crest cell cluster (Fig. S11B). Moreover, the cells of the pre-EMT neural crest cell cluster express roof plate markers, such as *Lmx1a*, *Msx1*, *Msx2* and *Wnt1* (Delile et al., 2019) (Fig. S12), suggesting that neural crest cells

Development (2022) 149, dev201052. doi:10.1242/dev.201052

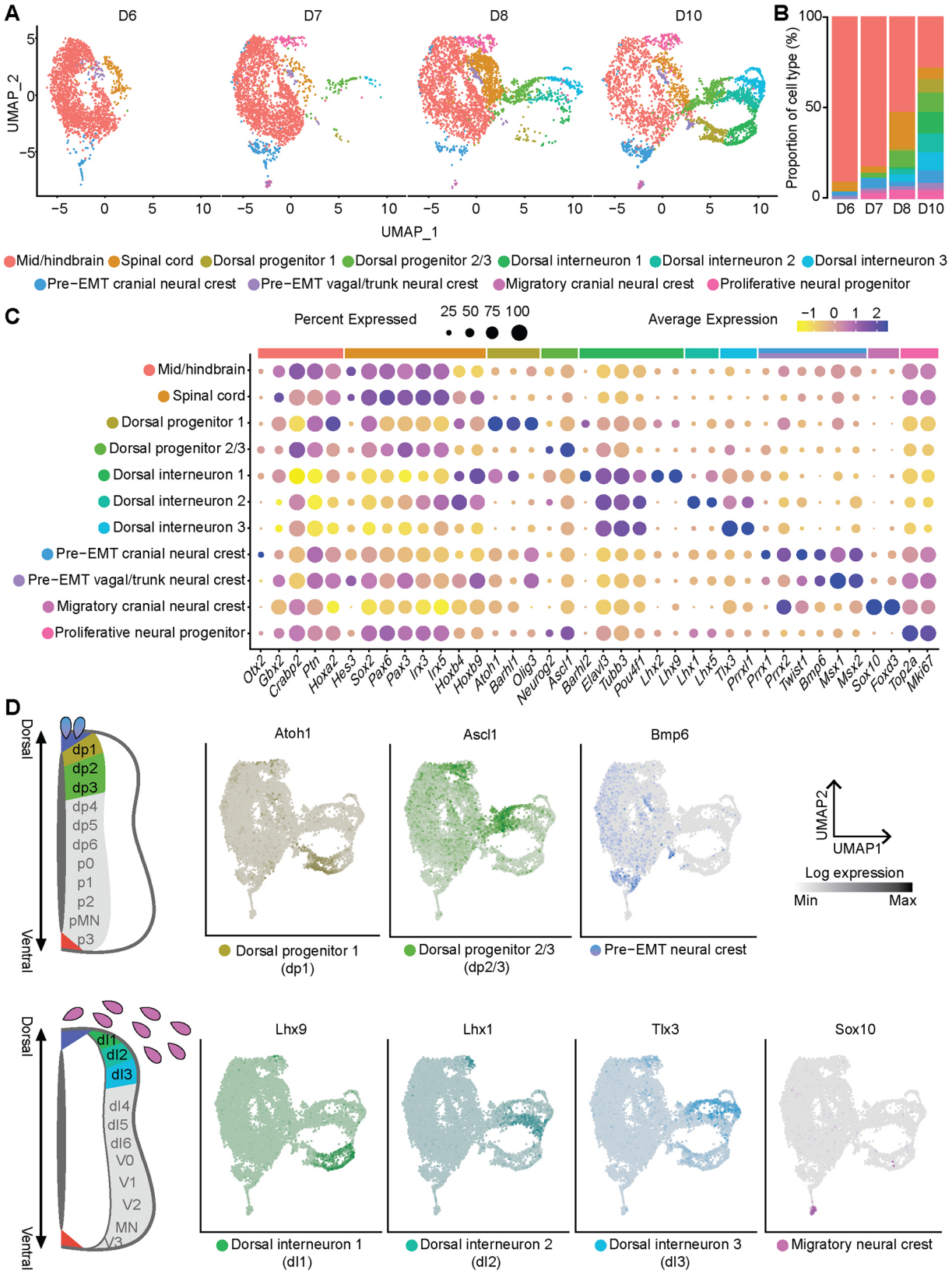

Fig. 4. See next page for legend.

arise from roof plate cells as *in vivo*. To the best of our knowledge, this is the first time such *in vivo*-like transcriptomic events of neural crest development have been detected in an *in vitro* model.

In addition, single-cell transcriptome analysis revealed neural differentiation in the mature neural tube organoid in detail. Consistent with the standard dorsal fate of the neural tube

Development (2022) 149, dev201052. doi:10.1242/dev.201052

Fig. 4. Single-cell transcriptomics captured the emergence of the neural crest and neural differentiation in mature neural tube organoids. (A) Single-cell RNA-sequence of the maturing organoids from D6 to D10 revealed 11 cell type clusters throughout the maturation, including dorsal progenitors, dorsal interneurons and neural crest cells (n=11,981 cells, N=1 biological sample for each timepoint). (B) The proportion of each cell type from D6 to D10 shows the evolvement of the neural tube organoids. On D6, the organoids were composed of mainly mid/hindbrain, spinal cord and pre-EMT cranial neural crest cells; from D7 and onwards, migratory cranial neural crest cells, dorsal progenitors and interneurons emerged from the organoid. (C) The key markers of each cell type are presented as a dot plot showing their average expression level and the percentage of expression in each cell type cluster. (D) The expression of the representative marker of each cell type was visualized on a UMAP projection identifying the dorsal progenitors, dorsal interneurons, pre-EMT neural crest cells and migratory neural crest cells: *Atoh1* for dorsal progenitor 1 (dp1), *Ascl1* for dorsal progenitor 2/3 (dp2/3), *Bmp6* for pre-EMT neural crest, *Lhx9* for dorsal interneuron 1 (dI1), *Lhx1* for dorsal interneuron 2 (dI2), *Tlx3* for dorsal interneuron 3 (dI3) and *Sox10* for migratory neural crest cells.

organoid, two identified neural progenitor clusters in mature neural tube organoids were the most dorsal progenitor domains of the neural tube: dorsal progenitor 1 (dp1) and dorsal progenitor 2/3 (dp2/3) (Fig. 4A,C). All of these progenitors collectively express the neural progenitor marker *Sox2* and are distinguished by their different markers: *Atoh1* and *Olig3* for dp1, and *Pax7* and *Ascl1* for dp2/3 (Fig. 4D, Fig. S13). These domains differentiate into dorsal interneurons: dp1 into dorsal interneuron 1 (dI1), and dp2/3 into dorsal interneuron 2 (dI2) and dorsal interneuron 3 (dI3). All dorsal interneuron clusters expressed both of the neuron markers *Tubb3* and *Elavl3*; dI1 neurons could be identified by the markers *Lhx2* and *Lhx9*, dI2 neurons by *Lhx1* and *Lhx5*, and dI3 neurons by *Tlx3* and *Prrxl1* (Fig. 4C,D, Fig. S13). Another marker for dorsal neurons, *Pou4f1* (also known as *Brn3a*), is also expressed in the dorsal interneuron clusters, and its expression was shown in the D10 organoid by immunofluorescence in Fig. 3D.

Overall, scRNAseq revealed the cell types and transcriptomic features of neural crest and neural development during maturation of the neural tube organoid. The migrating neural crest cells observed in the mature organoid were identified as cranial neural crest cells, and both cranial and vagal/trunk pre-EMT neural crest cells were detected. In addition, neurons in the mature organoid were identified as dorsal interneurons derived from dorsal neural progenitors. We believe that these results demonstrate that the neural tube organoid faithfully recapitulates the neural crest and neural development in the embryo.

DISCUSSION

Here, we present a novel organoid model that faithfully reproduces key features of the developing mouse embryonic neural tube, such as its elongated tubular architecture with a neural canal, AP patterning and the emergence of neural crest cells and neurons. Our system allows real-time observation of cell dynamics during morphogenesis and elongation, as well as patterning along the elongation axis with the emergence of region-specific cell identities.

A key parameter to promote self-elongation and -patterning in our model is the relatively low initial cell seeding density, which is ∼30% of that reported in previous neuronal cyst models (Meinhardt et al., 2014; Ranga et al., 2016). When stem cells are cultured at the cell density specified in previous neural cyst protocols, the tissue remains cystic, i.e. spontaneous expansion does not occur. The effect of cell density on organoid development should be further investigated.

Another intriguing aspect of our neural tube organoid is that AP-patterning occurs spontaneously, i.e. without 'artificial' posterization culture conditions induced by e.g. CHIR99021 or RA (Meinhardt et al., 2014; Ranga et al., 2016; Turner et al., 2017; Beccari et al., 2018; Veenvliet et al., 2020). For example, the generation of gastruloid or trunk-like structure (TLS) requires a CHIR99021 pulse that promotes emergence of $SOX2^{+}T/brachyury^{+}$ NMP-like cells that drive axial elongation of the system (Veenvliet et al., 2020), as in the tail bud *in vivo*. Reporter gene expression analysis, immunostaining and scRNAseq experiments do not indicate the presence of such NMP-like cells in our model. Considering that NMPs at the tail bud of the embryo contribute to secondary neurulation, forming the posterior spinal cord and expressing posterior Hox genes, and that our neural tube organoid lacks a NMP population and posterior Hox gene expression, we believe that elongation and AP patterning in our system occur via a different mechanisms (Copp et al., 2003; Deschamps and Duboule, 2017; Nikolopoulou et al., 2017).

Another important aspect of neural tube development is patterning along the DV axis. Our neural tube organoids have a default dorsal fate, as reported in previous studies (Meinhardt et al., 2014; Ranga et al., 2016). However, we have shown that the neural tube organoid responds to ventral morphogens and can differentiate into ventral cell types in response to the morphogens, in the same way that it does *in vivo*. This result highlights the potential of our organoid model for studying patterning and cell type derivation with morphogen gradients *in vitro*.

Finally, the accessibility of this system allows the emergence, delamination and migration of neural crest cells to be studied in real time. In particular, we could observe a phagocytosis event of migrating neural crest cells in real-time that has never been reported in a mammalian model due to its poor accessibility. As many neurocristopathies are caused by abnormalities in migration of neural crest cells, dissecting the migration of neural crest cells with this tractable system would allow us to better understand the mechanisms involved in these pathologies. We expect our organoids to open interesting avenues to the study of tissue mechanics, patterning, and neural crest and neural development in the mammalian neural tube at the cellular and molecular levels. Collectively, our system should contribute to understanding and facilitating the exploration of mammalian neural tube developmental processes and neurodevelopmental diseases in a tractable and potentially scalable manner.

MATERIALS AND METHODS

Culture of mouse embryonic stem cells

$Sox1^{eGFP}$;$Bra^{mCherry}$ double reporter (SBr; Deluz et al., 2016) mouse embryonic stem cells (mESCs) were used for the main experiments, except those shown in Fig. S2. Briefly, the mESC knock-in reporter line SBr was derived from CGR8 mouse ES cells with homology directed repair (HDR) and the fluorescent protein was cloned into Sox1 and Bra loci with 5′-P2A sequence. The cells were cultured in DMEM supplemented with 10% serum medium [10% ES-grade fetal bovine serum (FBS), 0.1 mM non-essential amino acids (NEAA), 1 mM sodium pyruvate, 3.44 mM GlutaMax, 0.1 mM β-mercaptoethanol (β-ME), 100 U/ml penicillin and 100 µg/ml streptomycin] with 2i (3 µM CHIR99021 and 1 µM PD025901) and 100 µg/ml LIF in a humidified incubator (5% CO_2, 37°C). The cells were split every other day, by washing with PBS (Gibco, 10010056) and dissociating with Accutase for 2 min at room temperature. The cell suspension was collected in a tube and centrifuged at 200 ***g*** for 5 min. After centrifugation, the cell pellet was resuspended in 1 ml of 10% serum medium and the cells were counted with a hemocytometer. 85,000 cells were plated in each well of a six-well plate (Corning) in 2 ml of 10% serum

Development (2022) 149, dev201052. doi:10.1242/dev.201052

medium with 2i and LIF and cultured in the humidified incubator. The cells were passaged every 2 days.

Neural tube organoid culture

mESCs were collected by washing with PBS and dissociating with Accutase for 2 min at room temperature. The cell suspension was collected in a centrifuge tube and was centrifuged at 200 ***g*** for 5 min. After centrifugation, the cell pellet was resuspended in 1 ml of 10% serum medium and the cells were counted with a hemocytometer. After cell counting, the cells were washed twice with PBS and were resuspended in N2B27 (47.4% Neurobasal medium, 47.4% DMEM/F-12 with 2.50 mM GlutaMAX, 1 mM GlutaMAX supplement, 100 U/ml penicillin, 100 µg/ml streptomycin, 0.1 mM NEAA, 1 mM sodium pyruvate, 0.1 mM β-ME, 1% B27 supplement and 0.5% N-2 supplement) and embedded in Matrigel to a final concentration of 1125 cells/10 µl drop of Matrigel for SBr. 10 µl of the resulting Matrigel-embedded cell suspension were deposited in each well of a 24-well plate (Corning). The cells in each well were cultured in 500 µl of Epi medium [N2B27 supplemented with 12 ng/ml basic fibroblast growth factor (bFGF, Thermofisher, PMG0031) and 20 ng/ml activin-A (R&D Systems, 338-AC-010)] for the first 3 days. On D3, the Epi medium of each well was substituted with 1 ml of N2B27. The medium of each well was substituted with 1 ml of N2B27 on D5 and the cells were cultured until D6. To test the reproducibility of self-elongating neural tube organoid formation, we tested three other mESC lines: (1) wild-type of the SBr cell line (Deluz et al., 2016) (SBr wild type in Fig. S2), (2) *Sox1*^{GFP} mESCs (Aubert et al., 2003; Meinhardt et al., 2014) and (3) *Sox10*^{GFP} mESCs (Kawaguchi et al., 2010) (Fig. S2). All the cell lines were maintained and cultured following the same protocol except for the initial cell embedding density in the Matrigel drop on D0 (Table S1).

Maturation of neural tube organoids

To harvest the organoids, on D6, the Matrigel drops with organoids were washed once with PBS and then treated with 3 mg/ml collagenase IV and 1 mg/ml dispase in HBSS+/+ for 30 min on a shaker to dissolve the Matrigel. After Matrigel was dissolved, the organoids were collected with cut 1000 µl pipette tips coated with 10% serum and centrifuged at 150 ***g*** for 5 min. The supernatant was removed and the organoids were suspended in N2B27 medium. The organoids were collected and re-embedded in 10 µl of Matrigel (1 organoid/drop), plated on glass-bottomed 96-well plate and further cultured in 100 µl of N2B27 medium in 5% CO_2 and 37°C incubator, and the medium was changed every day.

Immunostaining and confocal microscopy

The organoids were collected from Matrigel drop by washing with PBS and dissolving the Matrigel using 4 mg/ml collagenase-IV and 100 µg/ml dispase I in HBSS+/+ on a shaker in the incubator for 40 min. The organoids were fixed in 4% paraformaldehyde (PFA) in PBS for 30 min at room temperature. The organoids were washed three times with PBS for 20 min each, permeabilized in 0.2% Triton X-100 in PBS for 1 h and blocked in blocking solution [3% bovine serum albumin (BSA) and 0.01% Triton X-100 in PBS] for 3 h to overnight. Primary antibody (Tables S3, S5) solution was prepared in Blocking solution, with 2 µg/ml of DAPI. The organoids were stained overnight on a low-speed orbital shaker at 4°C. The organoids were thoroughly washed with PBS every 30 min for 4 h. Secondary antibody (Tables S4, S5) solution was prepared, treated and washed the same way as primary antibody solution. Here, the immunostaining was processed to avoid the green channel apart from SOX1 antibody because there are always SOX1-GFP^{+} cell populations in the organoid. Elsewhere, it was processed in the far-red channel or red channel, as there are no brachyury-mCherry^{+} cells in the organoid (Fig. S5A). Thus, the color of the immunostaining images in the figures do not necessarily match the color of the channel for the secondary antibody that was used for the staining. Confocal images of organoids were generated using LSM700 (Zeiss) on an inverted Zeiss AxioObserver Z1 (Bioimaging and Optics Core Facility, EPFL), equipped with 10×/0.30 air, 20×/0.80 air and 63×/1.40 oil objectives, 405 nm, 488 nm, 555 nm and 639 nm lasers, and controlled by ZEN 2010 imaging software (Zeiss). Images were analyzed using FIJI (NIH).

Light-sheet microscopy

The organoids were collected, fixed and immunostained following the immunostaining method described above. CUBIC-mount [sucrose (250 g of 50%, w/v), 125 g urea (25%, w/v) and 125 g N,N,N′,N′-tetrakis (2-hydroxypropyl)ethylenediamine (25%, w/v) dissolved in 150 ml of distilled H_2O and brought up to 500 ml (Lee et al., 2016)] was diluted with water to reach a refractive index of 1.453. The organoids were embedded in 1% agarose solution in a 1.5 mm diameter capillary (701908) using a plunger and were cooled in 4°C to allow for agarose gelation. The glass capillaries with agarose-embedded organoids were dipped in CUBIC-mount overnight in a dark room at room temperature for tissue clearing. For imaging, the glass capillary with sample was mounted with sample holder and inserted into the Top-fed Zeiss Lightsheet Z1. The cell chamber was filled with CUBIC-mount solution and the organoids in the capillary were located in the field of view using the plunger. Images were acquired with a 20×/1.0 corr water W Plan Apochromat objective (for non-cleared samples) or a 20×/1.45 corr clearing EC Plan Neofluar objective (for cleared samples). DAPI, Alexa Fluor 488, Alexa Fluor 568 and Alexa Fluor 633 were excited with 405, 488, 555 and 639-nm lasers, respectively. Images were analyzed using IMARIS (Oxford Instruments) and FIJI (NIH).

Time-lapse imaging

To observe how the organoid and its lumen elongate between D4 and D6, the organoids of each well were treated with 1 ml of N2B27 with 500 nM Sir-actin (Table S5) for 4 h before imaging. Time-lapse images were acquired using either a Nikon Eclipse Ti inverted microscope system [equipped with a 10×/0.30 air objective, 632-nm filters, DS-Qi2 and Andor iXon Ultra DU888U (Oxford Instruments) cameras and controlled by NIS-Elements AR 5.11.02 (Nikon) software] or a Visitron CSU-W1 (equipped with a U PLAN S APO 60×/1.42 oil objective, sdc Cy5 filter, 50 µm Spinning Disk, ImagEMX2 camera and controlled by VisiView software) and a 647 nm laser for Sir-actin signal and bright-field illumination. The image was captured every hour between D4 and D6 (Nikon Eclipse Ti) or every 5 min between D5 and D6 (Visitron). Temperature was maintained at 37°C with 5% CO_2.

Quantitative analysis of axial elongation of the neural tube organoids

Time-lapse images were analyzed using FIJI. Bright-field images of organoids were segmented by thresholding and the Max Inscribed Circles function (FIJI function developed by O. Burri and R. Guiet, BIOP, EPFL) was used to fit circles in the segmented object. Axial length was determined by connecting the centers of the fitted circles. Elongation index was calculated by dividing axial length by the diameter of the largest inscribed circle determined by the Max Inscribed Circles function.

Gene expression analysis by quantitative PCR

The collected organoids were washed with PBS and resuspended in lysis buffer. RNA was extracted immediately using the RNAeasy micro kit (Qiagen, 74004) according to the manufacturer instructions with on-column DNase I (Qiagen) digestion. The extracted RNA concentration was measured using NanoDrop. cDNA was synthesized using the iScript cDNA Synthesis Kit (BioRad, 170-8891) according to the manufacturer's instructions using 1 µg of RNA of each sample replicate in a BioRad thermocycler. Quantitative PCR analysis of mRNA levels for the genes on primer list was performed using Power SYBR Green PCR Master Mix (ThermoFisher Scientific, 4367659) on the Applied Biosystems Quantstudio 6 Flex Real-Time PCR system. PCR primers were designed using NCBI Primer-Blast software (Table S2). Expression values of each gene were normalized to the Gapdh expression value of each sample replicate using the ΔΔCT method. The graph was plotted using Prism 8 (GraphPad) and error bars represent the s.d. across three biological replicate samples.

Sample preparation for single-cell RNA sequencing

The sample preparation was performed according to the instructions from 10X Genomics Single Cell Protocols (10X Genomics), with some

Development (2022) 149, dev201052. doi:10.1242/dev.201052

modification. The collected organoids (100 organoids per condition) were washed twice with PBS and trypsinized with TrypLE Express (Gibco, 12605-028) for 7 min in 37°C. The organoids were dissociated into single cells by pipetting up and down with a 1000 µl pipette tip, strained using 40 µm cell strainer and collected in a 1.5 µl microcentrifuge tube. Those single cells were centrifuged at 300 ***g*** for 5 min and resuspended in 1 ml of PBS with 0.04% BSA after removing the supernatant. The cell concentration was then determined. After the same centrifugation step was repeated, the cells were resuspended in PBS with 0.04% BSA to achieve a final cell concentration of 1 million cells/ml. After the trypsinization, the cells were always placed on ice.

Single-cell RNA sequencing

Single-cell transcriptomics profiling derived from the organoids from different timepoints (D6, D7, D8 and D10) was carried out using Chromium Single Cell Gene Expression (10X Genomics), according to the manufacturer's recommendations. Cellular suspension was loaded on a Chromium Controller instrument to generate Gel Beads-in-emulsion (GEMs), containing single cells. Reverse transcription and library preparation were performed using the Single Cell 3′ Reagent Kit v3 (10X Genomics), following the 10X Genomics protocol. The cells were sequenced at an average depth of 85,000 reads per cell.

Single cell RNA sequencing data analysis

Single cell RNA sequencing data analysis was performed using Seurat 4.1.0 (Stuart et al., 2019) on R, with raw feature-barcode matrices of the organoids from different timepoints (D6, D7, D8 and D10). Genes expressed in fewer than three cells and the cells with less than 200 features expressed were removed. Cells with unique feature counts between 3000 and 10,000, and less than 10% mitochondrial counts were used for analysis. Expression level was log normalized, and the top 2000 variable genes were calculated using the Variance Stabilizing Transformation (VST) algorithm. The datasets were integrated using 'FindIntegrationAnchors' and 'IntegrateData' function, and normalized by the 'LogNormalize' method with the dimension of 1:30 from CCA to specify the neighbor search space. After the integration, the effects of the batch ID, cell cycle, nUMI and mitochondrial counts were determined by regression analysis. The number of cells after filtering was 2076 (D6, self-elongating neural tube organoid replicate 1), 2402 (D6, self-elongating neural tube organoid replicate 2), 2225 (D6 NE, non-elongating neural tube organoid), 2565 (D7), 3337 (D8) and 3677 (D10). We scaled the data by applying a linear transformation and performed principal component analysis (PCA) on the scaled data. Clusters of cells were identified by a shared nearest neighbor (SNN) modularity optimization-based Louvain algorithm with a resolution of 1.0 (Waltman and van Eck, 2013). Clusters were visualized on a two-dimensional Uniform Manifold Approximation and Projection (UMAP) (Mcinnes et al., 2018 preprint). The cell type of each cluster was identified based on the markers of each cluster expressing more than 0.25 $\log_2$ fold-change different over the others. To estimate RNA velocity of each cell, velocyto.py (La Manno et al., 2018) was used to generate loom files for each dataset from D6 to D10 to be used for Seurat analysis. To do so, the bam file of each dataset produced by Cell Ranger (10X Genomics) and the gtf file from 10X Genomics were used for annotation. To integrate the loom file and the Seurat object in R, metadata-like filtered cell IDs, UMAP coordinates and clusters were extracted. Once the loom files were generated, the loom files and the metadata were integrated, and RNA velocity could be estimated based on the same UMAP coordinates and clusters using scVelo (Bergen et al., 2020) on Python. For cell type identification, we have referenced mainly two single cell transcriptomic analysis reports in the developing mouse neural tube: spatial and temporal dynamics of gene expression in spinal cord (Delile et al., 2019), and neural crest development (Soldatov et al., 2019).

Whole-mount single-molecule fluorescence *in situ* hybridization (smFISH)

20 nt fluorescently labeled DNA probes for detecting *Otx2*, *Gbx2*, *Hoxb1* and *Hoxb9* transcripts were designed and ordered according to Stellaris (LGC Biosearch) instructions (Table S6). The probes were resuspended in 1× TE buffer [10 mM Tris-HCl and 1 mM EDTA (pH 8.0] to stock concentration 12.5 µM and aliquoted. The organoids were collected, washed once in 1× PBS and fixed in 4% PFA for 30 min. Next, whole-mount organoids were placed on SuperFrost slides (ThermoFisher Scientific) in a drop of 1× PBS. After the buffer was evaporated (~30 min), organoids were attached to the slide for whole-mount staining. The organoids were permeabilized overnight in 70% ethanol at 4°C. An ImmEdge PAP pen (Vector laboratories) was used for creating a hydrophobic barrier around areas of interest. Next, the organoids were washed with 2× SSC twice. The tissue was incubated with smFISH hybridization buffer [2× SSC (Sigma Aldrich), 10% (w/v) dextran sulfate (Sigma Aldrich), 10% (v/v) Formamide (Ambion), 1 mg/ml *E. coli* tRNA (Roche) and 2 mM ribonucleoside vanadyl complexes (RVC) (Sigma Aldrich)] for 5 min without probes for buffer substitution. smFISH probes were resuspended in smFISH hybridization buffer to a final concentration of 250 nM to create the hybridization mix. Hybridization mix was incubated with the tissue for 4 h at 37°C in humidified environment. After hybridization, the tissue was washed three times for 10 min each with 20% formamide in 2× SSC at 37°C. Hoechst 33342 (ThermoFisher Scientific) staining was applied on the second wash to visualize nuclei. Next, the slides were washed twice with 2× SSC. The slides were mounted with ProLong Gold mounting media and imaged with an Upright Leica DM6 CS in wide-field imaging mode equipped with a DFC 7000 GT (CCD Grayscale) camera and a HC PL APO 40×/63× objective, and the following filters were used: DAPI (BP 350/50 excitation, BP 460/50 emission), RHOD (BP 546/10 excitation, BP 585/40 emission) and Y5 (BP 620/60 excitation, BP700/75 emission). To detect the smFISH spots in the image, an ImageJ plug-in RS-FISH (https://github.com/PreibischLab/RS-FISH) was used.

Statistics

All data shown in column graphs are expressed as mean±s.d. Statistical analysis between two columns was performed using a two-tailed unpaired Student's *t*-test, whereas data containing more than two experimental groups were analyzed with one-way ANOVA followed by Tukey's multiple comparisons test or with two-way ANOVA followed by Šídák's multiple comparisons test. Statistical significance was calculated using the Graphpad Prism software, which was also used to generate all the graphs. *P<0.05; **P<0.01; ***P<0.001; ****P<0.0001 (confidence intervals 95%; alpha level 0.05).

Acknowledgements

We thank R. Guiet and O. Burri of the BioImaging and Optics Core Facility (BIOP) for programming image-processing plug-in for elongation index quantification, and all the other staff for their help for the general support in imaging; all the staff from the Gene Expression Core Facility (GECF, EPFL) for their support on single-cell RNA sequencing (scRNAseq); S. Vianello, M. Leleu and N. Broguiere for the introduction to the scRNAseq analysis; A. Martinez Arias for help with defining cell types during scRNAseq analysis; G. Rossi for the introduction to Lightsheet fluorescence microscopy; and M. Girgin, S. Vianello, N. Brandenberg, A. Martinez Arias and E. Tanaka for the inputs on the manuscript. Some of the text and figures in this paper formed part of JiSoo Park's PhD thesis in the Doctoral Program in Biotechnology and Bioengineering (EDBB) at the Ecole Polytechnique Fédérale de Lausanne in 2021.

Competing interests

The authors declare no competing or financial interests.

Author contributions

Conceptualization: M.P.L., J.P.; Methodology: J.P.; Formal analysis: M.P.L., J.P.; Investigation: I.K., H.H.; Resources: M.P.L.; Data curation: J.P., H.H.; Writing - original draft: M.P.L., J.P.; Writing - review & editing: M.P.L., G.L.M.; Visualization: J.P.; Supervision: M.P.L.; Project administration: M.P.L.

Funding

This work was funded by the École Polytechnique Fédérale de Lausanne and a Schweizerischer Nationalfonds zur Förderung der Wissenschaftlichen Forschung Sinergia grant (3189956). Open Access funding provided by the École Polytechnique Fédérale de Lausanne. Deposited in PMC for immediate release.

Data availability

The scRNA-seq data discussed in this publication have been deposited in GEO under accession number GSE214996.

Peer review history
The peer review history is available online at https://journals.biologists.com/dev/lookup/doi/10.1242/dev.201052.reviewer-comments.pdf.

References

Aubert, J., Stavridis, M. P., Tweedie, S., O'reilly, M., Vierlinger, K., Li, M., Ghazal, P., Pratt, T., Mason, J. O., Roy, D. et al. (2003). Screening for mammalian neural genes via fluorescence-activated cell sorter purification of neural precursors from *Sox1 - gfp* knock-in mice. *Proc. Natl. Acad. Sci. USA* **100**, 11836-11841. doi:10.1073/pnas.1734197100

Bay, S. N. and Caspary, T. (2012). What are those cilia doing in the neural tube? *Cilia* **1**, 19. doi:10.1186/2046-2530-1-19

Baye, L. M. and Link, B. A. (2007). Interkinetic nuclear migration and the selection of neurogenic cell divisions during vertebrate retinogenesis. *J. Neurosci.* **27**, 10143-10152. doi:10.1523/JNEUROSCI.2754-07.2007

Beccari, L., Moris, N., Girgin, M., Turner, D. A., Baillie-Johnson, P., Cossy, A.-C., Lutolf, M. P., Duboule, D. and Arias, A. M. (2018). Multi-axial self-organization properties of mouse embryonic stem cells into gastruloids. *Nature* **562**, 272-276. doi:10.1038/s41586-018-0578-0

Bergen, V., Lange, M., Peidli, S., Wolf, F. A. and Theis, F. J. (2020). Generalizing RNA velocity to transient cell states through dynamical modeling. *Nat. Biotechnol.* **38**, 1408-1414. doi:10.1101/820936

Briscoe, J. and Small, S. (2015). Morphogen rules: design principles of gradient-mediated embryo patterning. *Development* **142**, 3996-4009. doi:10.1242/dev.129452

Brons, I. G. M., Smithers, L. E., Trotter, M. W. B., Rugg-Gunn, P., Sun, B., Chuva De Sousa Lopes, S. M., Howlett, S. K., Clarkson, A., Ahrlund-Richter, L., Pedersen, R. A. et al. (2007). Derivation of pluripotent epiblast stem cells from mammalian embryos. *Nature* **448**, 191-195. doi:10.1038/nature05950

Copp, A. J., Greene, N. D. E. and Murdoch, J. N. (2003). The genetic basis of mammalian neurulation. *Nat. Rev. Genet.* **4**, 784-793. doi:10.1038/nrg1181

Delile, J., Rayon, T., Melchionda, M., Edwards, A., Briscoe, J. and Sagner, A. (2019). Single cell transcriptomics reveals spatial and temporal dynamics of gene expression in the developing mouse spinal cord. *Development* **146**, dev173807. doi:10.1242/dev.173807

Deluz, C., Friman, E. T., Strebinger, D., Benke, A., Raccaud, M., Callegari, A., Leleu, M., Manley, S. and Suter, D. M. (2016). A role for mitotic bookmarking of SOX2 in pluripotency and differentiation. *Genes Dev.* **30**, 2538-2550. doi:10.1101/gad.289256.116

Demers, C. J., Soundararajan, P., Chennampally, P., Cox, G. A., Briscoe, J., Collins, S. D. and Smith, R. L. (2016). Development-on-chip: *in vitro* neural tube patterning with a microfluidic device. *Development* **143**, 1884-1892. doi:10.1242/dev.126847

Deschamps, J. and Duboule, D. (2017). Embryonic timing, axial stem cells, chromatin dynamics, and the Hox clock. *Genes Dev.* **31**, 1406-1416. doi:10.1101/gad.303123.117

Deschamps, J. and Van Nes, J. (2005). Developmental regulation of the Hox genes during axial morphogenesis in the mouse. *Development* **132**, 2931-2942. doi:10.1242/dev.01897

Dupin, E. (2006). *Neural Crest Induction and Differentiation* (ed. J.-P. Saint-Jeannet). New York, N.Y: Georgetown, Tex: Springer Science+Business Media; Landes Bioscience/Eurekah.com (Advances in experimental medicine and biology, v. 589).

Duval, N., Vaslin, C., Barata, T. C., Frarma, Y., Contremoulins, V., Baudin, X., Nedelec, S. and Ribes, V. C. (2019). BMP4 patterns Smad activity and generates stereotyped cell fate organization in spinal organoids. *Development* **146**, dev175430. doi:10.1242/dev.175430

Fame, R. M. and Lehtinen, M. K. (2020). Emergence and developmental roles of the cerebrospinal fluid system. *Dev. Cell* **52**, 261-275. doi:10.1016/j.devcel.2020.01.027

Fame, R. M., Cortés-Campos, C. and Sive, H. L. (2020). Brain ventricular system and cerebrospinal fluid development and function: light at the end of the tube: a primer with latest insights. *BioEssays* **42**, 1900186. doi:10.1002/bies.201900186

Greene, N. D. E. and Copp, A. J. (2009). Development of the vertebrate central nervous system: formation of the neural tube. *Prenat. Diagn.* **29**, 303-311. doi:10.1002/pd.2206

Hayashi, K., Ohta, H., Kurimoto, K., Aramaki, S. and Saitou, M. (2011). Reconstitution of the mouse germ cell specification pathway in culture by pluripotent stem cells. *Cell* **146**, 519-532. doi:10.1016/j.cell.2011.06.052

Huch, M., Knoblich, J. A., Lutolf, M. P. and Martinez-Arias, A. (2017). The hope and the hype of organoid research. *Development* **144**, 938-941. doi:10.1242/dev.150201

Kawaguchi, J., Nichols, J., Gierl, M. S., Faial, T. and Smith, A. (2010). Isolation and propagation of enteric neural crest progenitor cells from mouse embryonic stem cells and embryos. *Development* **137**, 693-704. doi:10.1242/dev.046896

La Manno, G., Soldatov, R., Zeisel, A., Braun, E., Hochgerner, H., Petukhov, V., Lidschreiber, K., Kastriti, M. E., LÃ¶Nnerberg, P., Furlan, A. et al. (2018). RNA velocity of single cells. *Nature* **560**, 494-498. doi:10.1038/s41586-018-0414-6

Le Douarin, N. M., Creuzet, S., Couly, G. and Dupin, E. (2004). Neural crest cell plasticity and its limits. *Development* **131**, 4637-4650. doi:10.1242/dev.01350

Lee, E., Choi, J., Jo, Y., Kim, J. Y., Jang, Y. J., Lee, H. M., Kim, S. Y., Lee, H.-J., Cho, K., Jung, N. et al. (2016). ACT-PRESTO: rapid and consistent tissue clearing and labeling method for 3-dimensional (3D) imaging. *Sci. Rep.* **6**, 18631. doi:10.1038/srep18631

Libby, A. R. G., Joy, D. A., Elder, N. H., Bulger, E. A., Krakora, M. Z., Gaylord, E. A., Mendoza-Camacho, F., Butts, J. C. and Mcdevitt, T. C. (2021). Axial elongation of caudalized human pluripotent stem cell organoids mimics neural tube development. *Development* **148**, dev198275. doi:10.1242/dev.198275

Mcinnes, L., Healy, J. and Melville, J. (2018). UMAP: uniform manifold approximation and projection for dimension reduction. *arXiv:1802.03426* http://arxiv.org/abs/1802.03426 (Accessed: 8 June 2020).

Meinhardt, A., Eberle, D., Tazaki, A., Ranga, A., Niesche, M., Wilsch-Bräuninger, M., Stec, A., Schackert, G., Lutolf, M. and Tanaka, E. M. (2014). 3D reconstitution of the patterned neural tube from embryonic stem cells. *Stem Cell Rep.* **3**, 987-999. doi:10.1016/j.stemcr.2014.09.020

Miyata, T., Okamoto, M., Shinoda, T. and Kawaguchi, A. (2015). Interkinetic nuclear migration generates and opposes ventricular-zone crowding: insight into tissue mechanics. *Front. Cell. Neurosci.* **8**, 473. doi:10.3389/fncel.2014.00473

Nikolopoulou, E., Galea, G. L., Rolo, A., Greene, N. D. E. and Copp, A. J. (2017). Neural tube closure: cellular, molecular and biomechanical mechanisms. *Development* **144**, 552-566. doi:10.1242/dev.145904

Ogura, T., Sakaguchi, H., Miyamoto, S. and Takahashi, J. (2018). Three-dimensional induction of dorsal, intermediate and ventral spinal cord tissues from human pluripotent stem cells. *Development* **145**, dev162214. doi:10.1242/dev.162214

Pilon, N. (2021). Treatment and prevention of neurocristopathies. *Trends Mol. Med.* **27**, 451-468. doi:10.1016/j.molmed.2021.01.009

Ranga, A., Girgin, M., Meinhardt, A., Eberle, D., Caiazzo, M., Tanaka, E. M. and Lutolf, M. P. (2016). Neural tube morphogenesis in synthetic 3D microenvironments. *Proc. Natl. Acad. Sci. USA* **113**, E6831-E6839. doi:10.1073/pnas.1603529113

Rifes, P., Isaksson, M., Rathore, G. S., Aldrin-Kirk, P., MÃ¸Ller, O. K., Barzaghi, G., Lee, J., Egerod, K. L., Rausch, D. M., Parmar, M. et al. (2020). Modeling neural tube development by differentiation of human embryonic stem cells in a microfluidic WNT gradient. *Nat. Biotechnol.* **38**, 1265-1273. doi:10.1038/s41587-020-0525-0

Rossi, G., Manfrin, A. and Lutolf, M. P. (2018). Progress and potential in organoid research. *Nat. Rev. Genet.* **19**, 671-687. doi:10.1038/s41576-018-0051-9

Sadler, T. W. (2005). Embryology of neural tube development. *Am. J. Med. Genet. C Semin. Med. Genet.* **135C**, 2-8. doi:10.1002/ajmg.c.30049

Sagner, A. and Briscoe, J. (2017). Morphogen interpretation: concentration, time, competence, and signaling dynamics: morphogen interpretation. *Wiley Interdiscip. Rev. Dev. Biol.* **6**, e271. doi:10.1002/wdev.271

Sagner, A. and Briscoe, J. (2019). Establishing neuronal diversity in the spinal cord: a time and a place. *Development* **146**, dev182154. doi:10.1242/dev.182154

Sato, T. S., Handa, A., Priya, S., Watal, P., Becker, R. M. and Sato, Y. (2019). Neurocristopathies: enigmatic appearances of neural crest cell-derived abnormalities. *Radiographics* **39**, 2085-2102. doi:10.1148/rg.2019190086

Schilling, T. F. (2008). Anterior-posterior patterning and segmentation of the vertebrate head. *Integr. Comp. Biol.* **48**, 658-667. doi:10.1093/icb/icn081

Soldatov, R., Kaucka, M., Kastriti, M. E., Petersen, J., Chontorotzea, T., Englmaier, L., Akkuratova, N., Yang, Y., HÃ¤Ring, M., Dyachuk, V. et al. (2019). Spatiotemporal structure of cell fate decisions in murine neural crest. *Science* **364**, eaas9536. doi:10.1126/science.aas9536

Stuart, T., Butler, A., Hoffman, P., Hafemeister, C., Papalexi, E., Mauck, W. M., Hao, Y., Stoeckius, M., Smibert, P. and Satija, R. (2019). Comprehensive integration of single-cell data. *Cell* **177**, 1888-1902.e21. doi:10.1016/j.cell.2019.05.031

Takebe, T. and Wells, J. M. (2019). Organoids by design. *Science* **364**, 956-959. doi:10.1126/science.aaw7567

Thouvenin, O., Keiser, L., Cantaut-Belarif, Y., Carbo-Tano, M., Verweij, F., Jurisch-Yaksi, N., Bardet, P.-L., Van Niel, G., Gallaire, F. and Wyart, C. (2020). Origin and role of the cerebrospinal fluid bidirectional flow in the central canal. *Elife* **9**, e47699. doi:10.7554/eLife.47699

Turner, D. A., Girgin, M., Alonso-Crisostomo, L., Trivedi, V., Baillie-Johnson, P., Glodowski, C. R., Hayward, P. C., Collignon, J., Gustavsen, C., Serup, P. et al. (2017). Anteroposterior polarity and elongation in the absence of extra-embryonic tissues and of spatially localised signalling in gastruloids: mammalian embryonic organoids. *Development* **144**, 3894-3906. doi:10.1242/dev.150391

Veenvliet, J. V., Bolondi, A., Kretzmer, H., Haut, L., Scholze-Wittler, M., Schifferl, D., Koch, F., Pustet, M., Heimann, S., Buschow, R. et al. (2020). Mouse embryonic stem cells self-organize into trunk-like structures with neural tube and somites. *Science* **370**, eaba4937. doi:10.1126/science.aba4937 doi:10.1101/2020.03.04.974949

Vega-Lopez, G. A., Cerrizuela, S., Tribulo, C. and Aybar, M. J. (2018). Neurocristopathies: new insights 150 years after the neural crest discovery. *Dev. Biol.* **444**, S110-S143. doi:10.1016/j.ydbio.2018.05.013

Waltman, L. and Van Eck, N. J. (2013). A smart local moving algorithm for large-scale modularity-based community detection. *Eur. Phys. J. B* **86**, 471. doi:10.1140/epjb/e2013-40829-0

Yamaguchi, T. P. (2001). Heads or tails: Wnts and anterior–posterior patterning. *Curr. Biol.* **11**, R713-R724. doi:10.1016/S0960-9822(01)00417-1

Zheng, Y., Xue, X., Resto-Irizarry, A. M., Li, Z., Shao, Y., Zheng, Y., Zhao, G. and Fu, J. (2019). Dorsal-ventral patterned neural cyst from human pluripotent stem cells in a neurogenic niche. *Sci. Adv.* **5**, eaax5933. doi:10.1126/sciadv.aax5933

Zhu, Y., Crowley, S. C., Latimer, A. J., Lewis, G. M., Nash, R. and Kucenas, S. (2019). Migratory neural crest cells phagocytose dead cells in the developing nervous system. *Cell* **179**, 74-89.e10. doi:10.1016/j.cell.2019.08.001

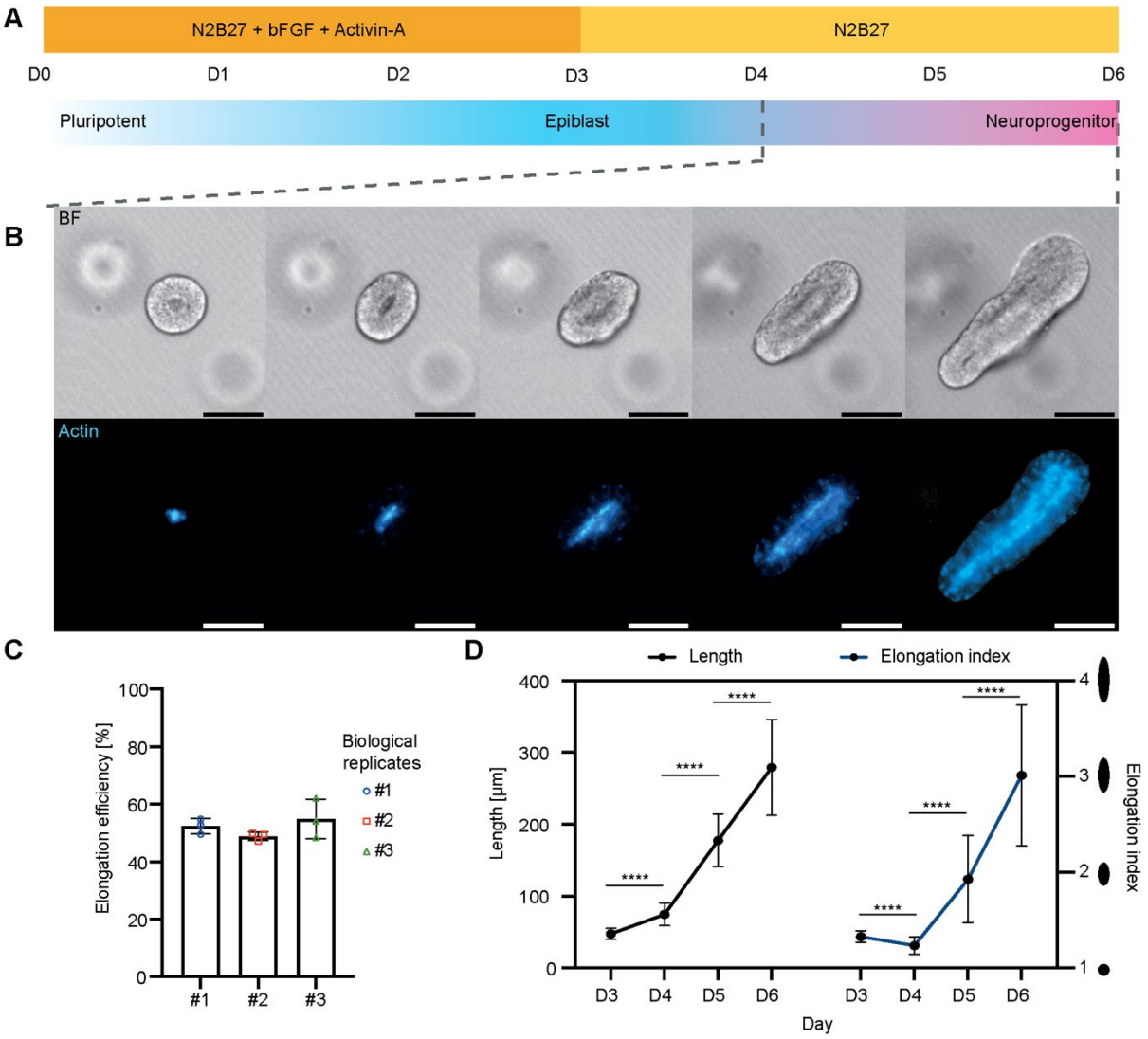

Fig. S1. **Generation of self-elongating neural tube organoids in 3D. A**, Schematic representation of self-elongating neural tube organoids culture in 3D. Single mouse ESCs embedded in Matrigel cultured in epiblast medium (N2B27 with Activin-A and bFGF) form epiblast-state cysts on D3. From D3 on, the medium was changed to N2B27 for neural differentiation. On D4, cysts undergo uniaxial elongation and form elongated neural tube-like structure bearing a single and continuous elongated lumen. **B**, Representative time-lapse images capturing the elongation of a neuroepithelial cyst into a tubular structure between D4 and D6. The images were obtained both in brightfield and fluorescence with a live cell actin probe to capture both the elongation of neuroepithelial cysts and their respective lumen. Surprisingly, the apicobasal polarization of the organoid was maintained during elongation. **C**, Elongation efficiency of neuroepithelial cyst of three independent biological replicates. **D**, Quantitative analysis of elongation in length as well as the Elongation index between D3 and D6. All the scale bars are 100 µm.

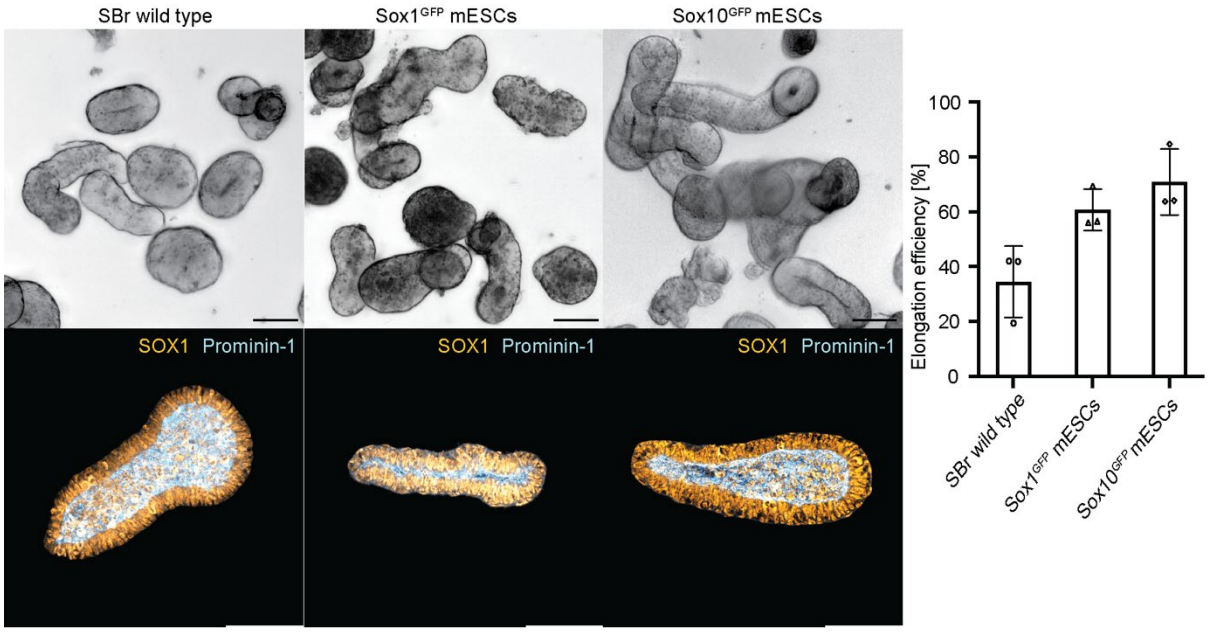

Fig. S2. Reproducible generation of self-elongating neural tube organoid across different cell lines. Self-elongating neural tube organoid could be generated in a reproducible manner in three different cell lines: Wild type of SBr cell line (Deluz *et al.*, 2016), *Sox1*^{GFP} mESCs (Aubert *et al.*, 2003; Meinhardt *et al.*, 2014) and *Sox10*^{GFP} mESCs (Kawaguchi *et al.*, 2010). Each cell line has its optimal Matrigel-embedding cell density (Table 1) and their efficiency of elongation is about 55.34 ±18.92% in average.

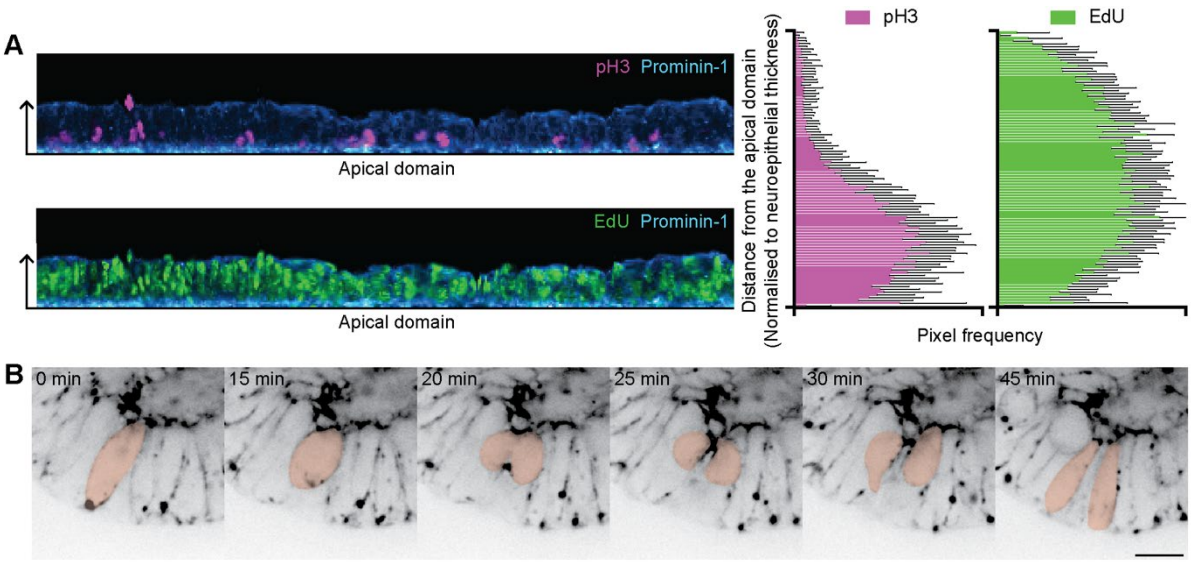

Fig. S3. Interkinetic nuclear migration is exhibited in the neural tube organoid. A, straightened image of epithelium of neural tube organoid stained against pH3 (M-phase cell) and EdU (S-phase cell) showed the apically localised M-phase mitotic cells. The quantification of the pixel frequency of $pH3^{+}$ or EdU^{+} signal along the thickness of the epithelium show the biased localisation of mitotic cells at the apical domain of the organoid (n=22). **B**, timelapse of the organoid stained with live actin could capture interkinetic nuclear migration and their cell division at the apical domain. Scale bar is 20 μm.

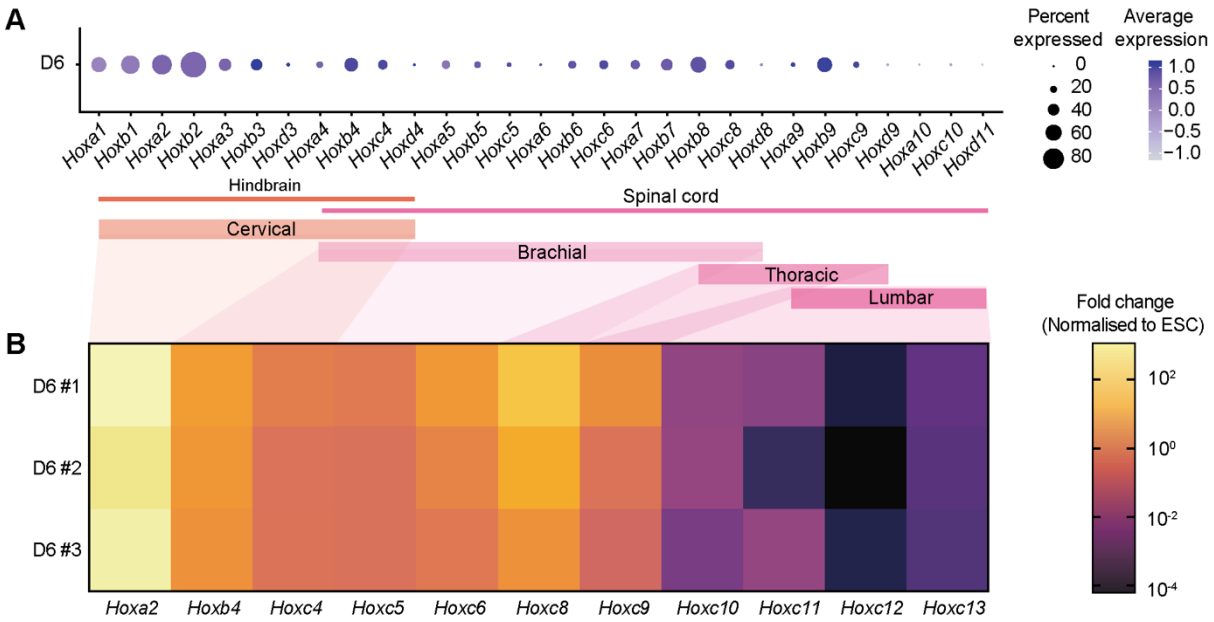

Fig. S4. Hox gene expression in neural tube organoid. A, Dot plot showing Hox genes and their expression level in neural tube organoids on D6. The percentage of cells expressing anterior Hox genes is larger but shows lower expression levels, whereas posterior Hox genes are expressed in fewer cells but these show higher expression level. The range of Hox gene expression spans between the cervical level (hindbrain) to the beginning of lumbar level (spinal cord). **B**, Reproducible Hox gene expression in three biological replicates of D6 neural tube organoids analyzed by qPCR also range from cervical to lumbar neural tube levels.

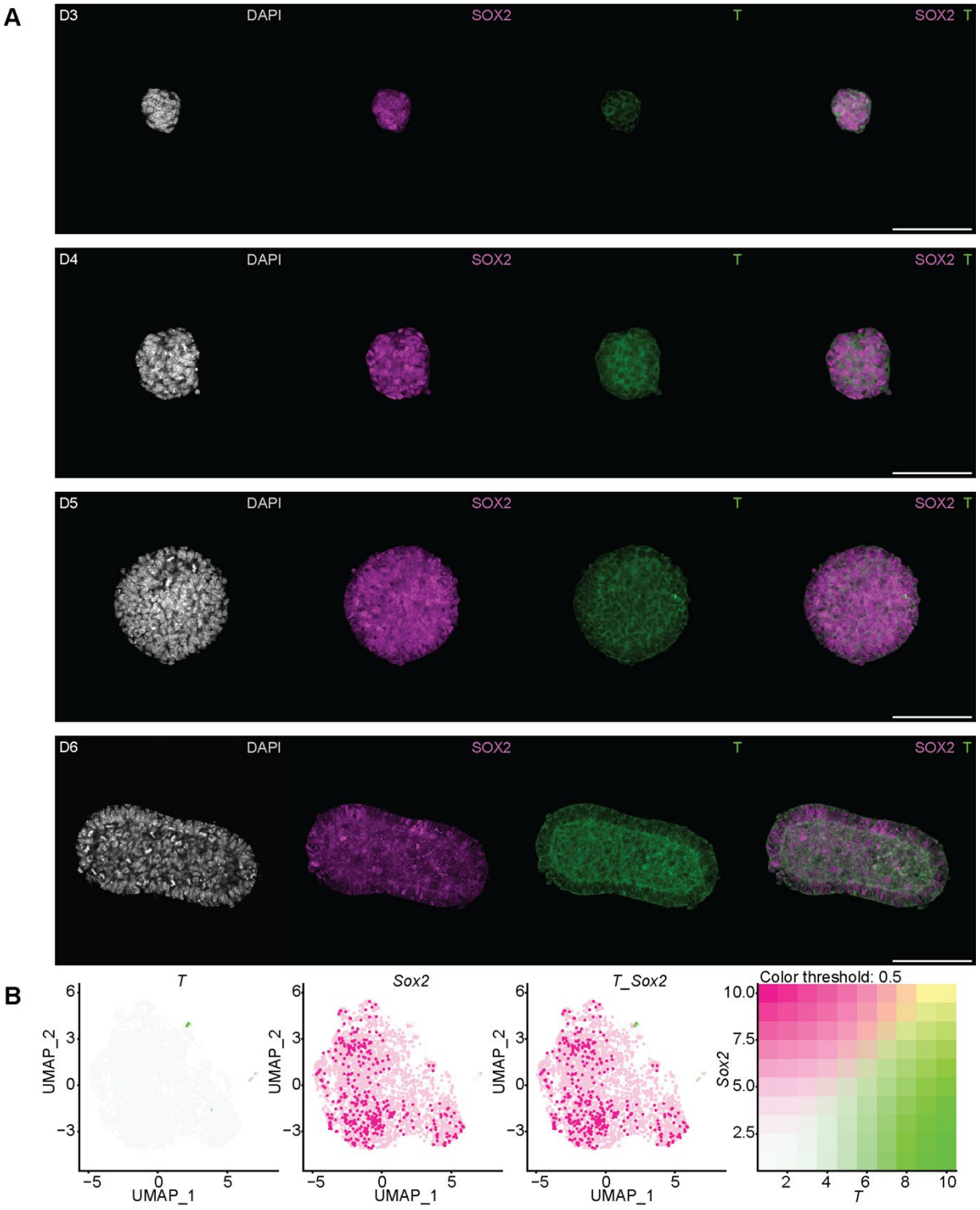

Fig. S5. Neuromesodermal progenitor (NMP) was not detected in neural tube organoid. A, Immunostaining of neural tube organoid against T (mesodermal) and SOX2 (neural) on D3 to D6 shows that there is no NMP (T^+ $SOX2^+$) detected in the organoid. **B**, scRNAseq analysis did not detect any NMP (T^+ $SOX2^+$) population in the organoid on D6. The UMAP plots were generated from the same data set analysis of Fig. 2.

Supplementary Figure 6

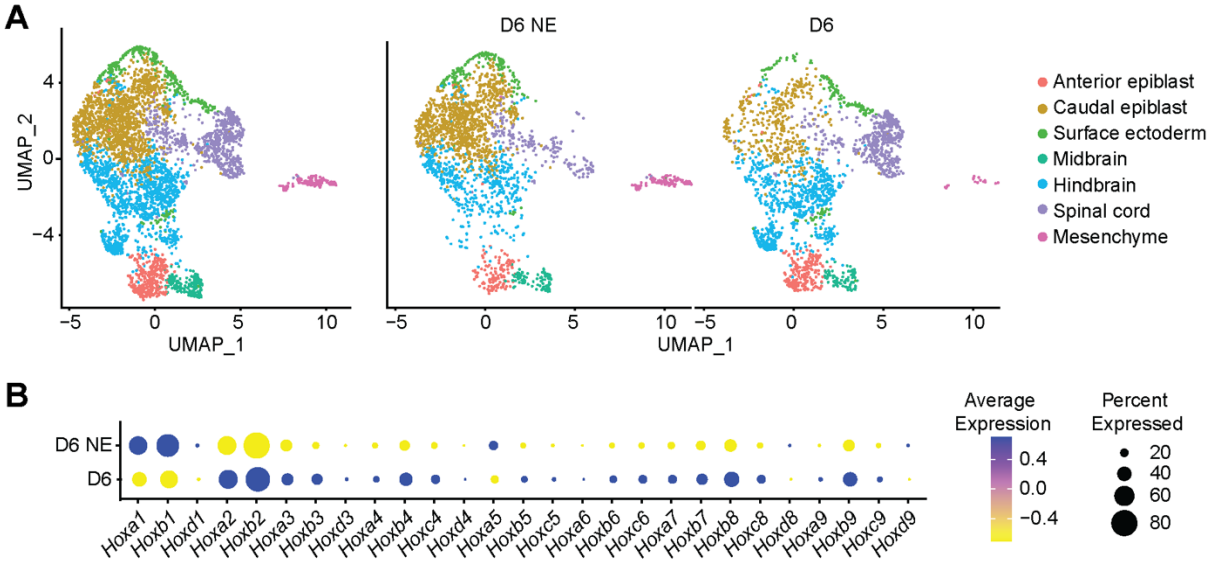

Fig. S6. Comparison between self-elongated neural tube organoid (D6) and non-elongated neural tube organoid (D6 NE) using scRNAseq. A, D6 and D6 NE shares all the cell types but the neural progenitors with spinal cord identity are preferentially found in self-elongated organoid. **B**, Dotplot of Hox genes along AP axis shows that D6 organoids express Hox genes along the AP axis from Hox2 level to Hox9 level while D6 NE organoids express anterior Hox gene restrictedly.

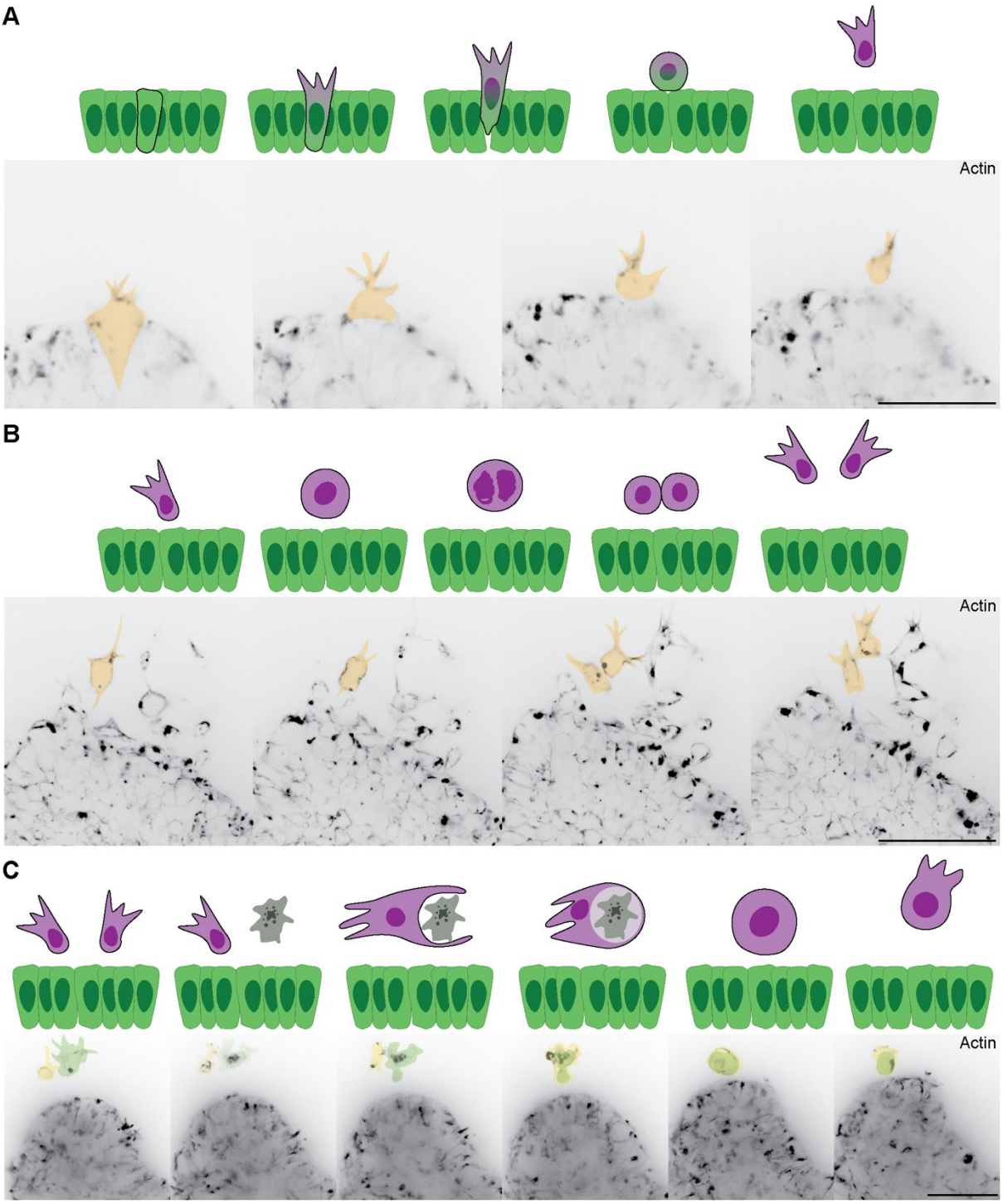

Fig. S7. Real-time observation of neural crest cell emergence. A, Delamination and migration of neural crest cells. The schematic and the time-lapse images depict the process of delamination and migration of the neural crest cells emerged from neural tube organoid. First, the cell protrudes out its filopodia out of the neuroepithelium and changes its morphology to go on the surface of the neuroepithelium. Then, the cell is entirely separated from the neural tube organoid and migrate away from the organoid having the filopodia towards the direction of migration. **B**, Self-renewal of migratory neural crest cells. The schematic and the time-lapse images show the self-renewal of migratory neural

crest cell. C, Phagocytosis of migrating neural crest cells. The schematic and the time-lapse images demonstrate the phagocytosis of migrating neural crest cells. When there was an apoptotic cell, the neighbouring migratory neural crest cell migrated towards the apoptotic debris, engulfed, and continued migrating. All the scale bars are 50 μm.

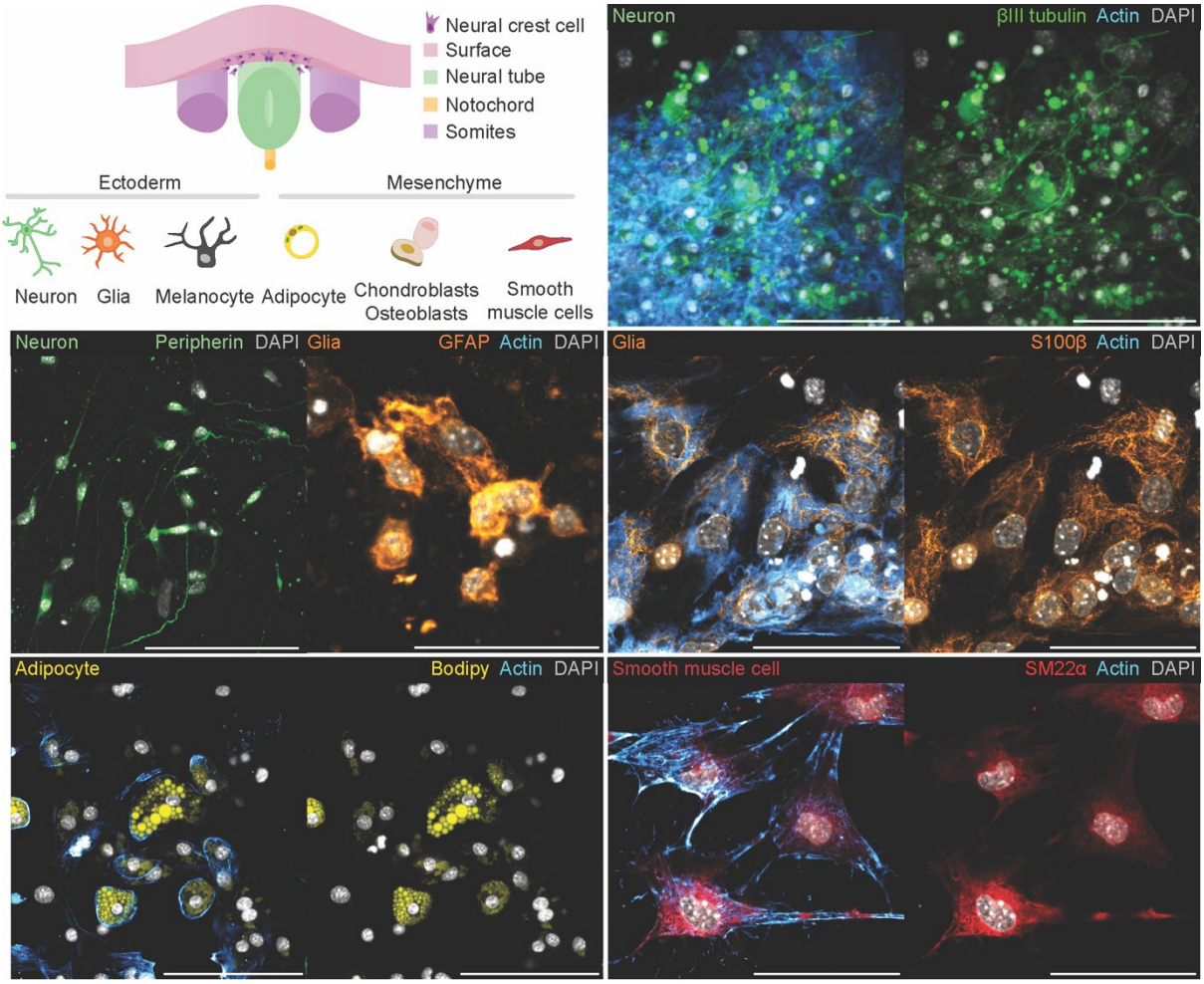

Fig. S8. Multipotency of neural crest cells derived from mature neural tube organoid. Neural crest cells can be derived into ectodermal cells, such as neuron and glia, and mesenchymal derivatives, such as adipocyte and smooth muscle cells. Culturing the neural tube organoid for a month revealed the multipotency of the neural crest cells. Confocal imaging confirmed that the neural crest cells have differentiated into various cell types: neurons expressing βIII tubulin, glial cells expressing GFAP and S100β, mesenchymal derivatives like adipocyte with the lipid droplets visualized by Bodipy and smooth muscle cells expressing SM22α. All the scale bars are 50 μm.

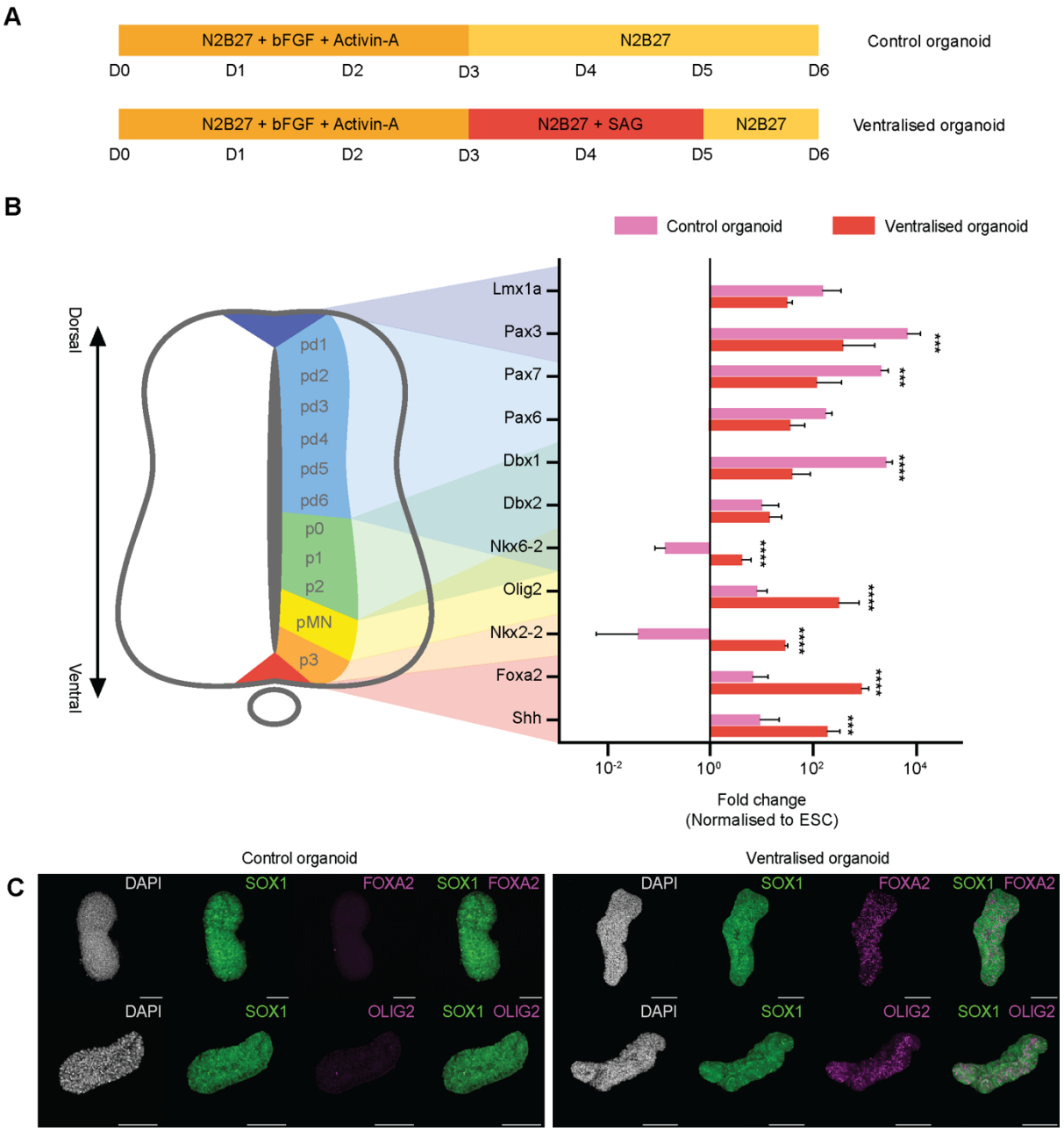

Fig. S9. Ventral morphogen can induce ventral identity cell types in the organoid. A, Schematic representation of the protocol used to ventralise the organoids. After culture in epiblast medium, control neuroepithelial cysts are cultured in N2B27 or in N2B27 with supplemented with 500 nM smoothened agonist (SAG, SHH signalling pathway activator) between D3 and D5 to ventralise the organoid. **B**, qPCR analysis of dorsal-ventral patterning markers of the embryonic neural tube, in control organoid and ventralised organoids. Control organoids show high expression of dorsal markers and low expression of ventral markers, while ventralised organoids show strong upregulation of ventral markers and also retain substantial expression of dorsal markers. This result shows that the organoid has default dorsal fate until ventral morphogen was treated. Values are mean ±SEM. Statistical analysis by 2-way ANOVA with Sidak's multiple comparisons test, ***p<0.001, ****p<0.0001. **C**, Confocal imaging revealed the predominant presence of ventral marker FOXA2 and OLIG2 at the protein level in ventralised organoids comparing to control organoids. This result suggests that selective dorsal or ventral fate of neural tube organoids can be obtained by following according culture condition. All the scale bars are 100 μm.

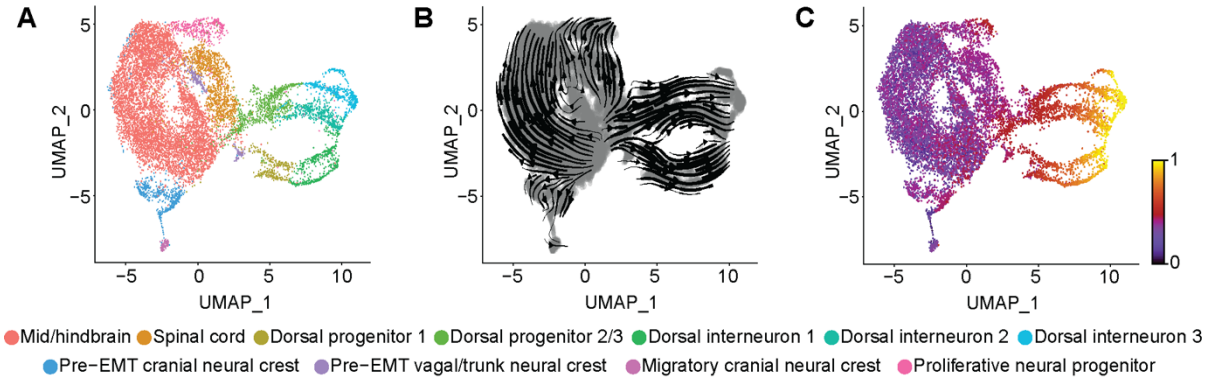

Fig. S10. RNA velocity analysis aligns with the maturation of the neural tube organoid. A, scRNAseq of the maturing organoids from D6 to D10 revealed 11 cell type clusters throughout the maturation including dorsal progenitors, dorsal interneurons, and neural crest cells (n= 11,981, N=1 biological sample for each timepoint). **B**, Streamline of RNA velocity displays the developmental process of maturation of neural tube organoid. **C**, Velocity pseudotime computed by RNA velocity aligns with temporal profile of the samples from D6 to D10 on UMAP projection. All the plots were generated from the same data set analysis of Fig. 4.

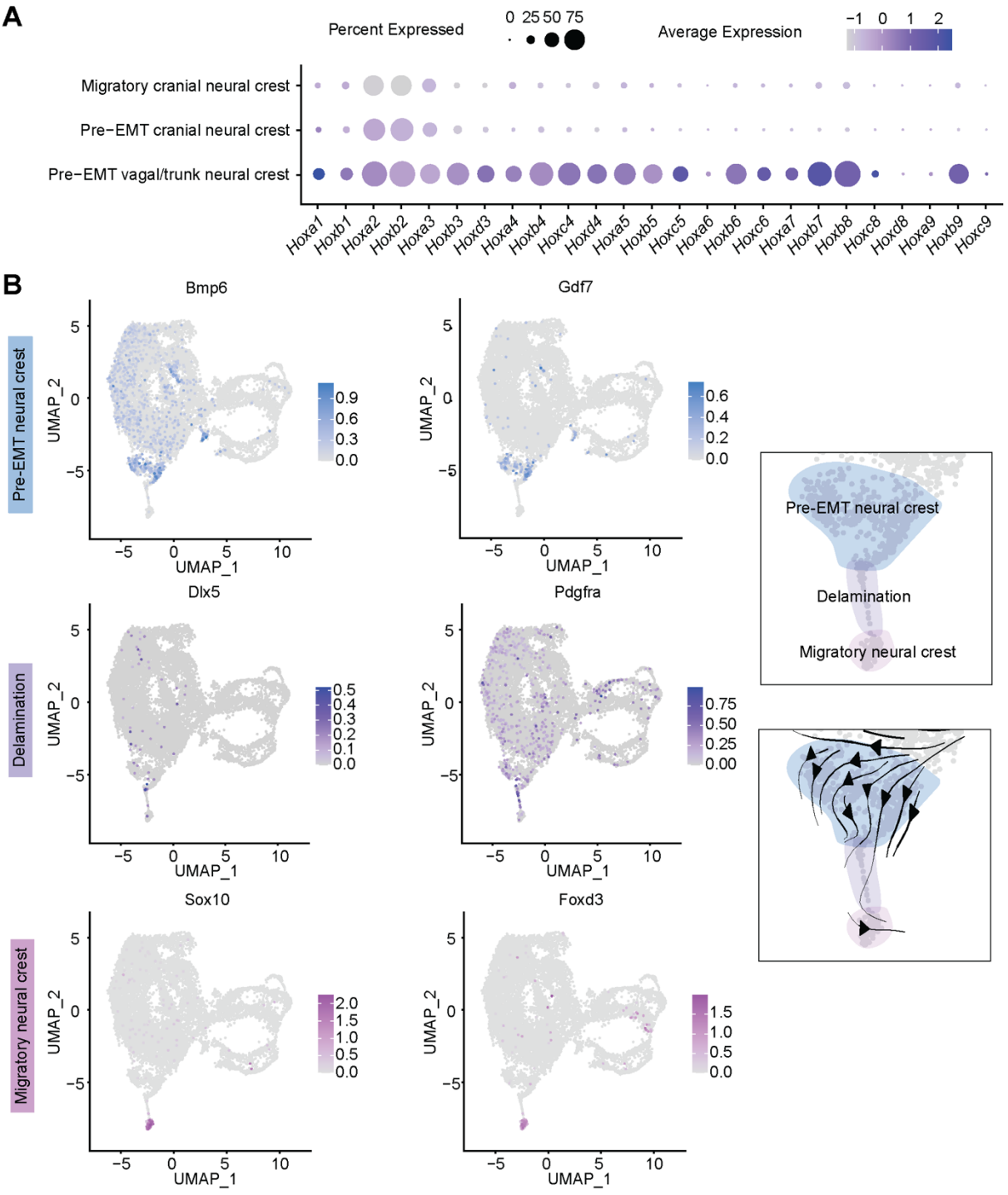

Fig. S11. scRNAseq analysis of mature neural tube organoids from different timepoint captured the transcriptomic event in neural crest cells from emergence to migration and their regional identity. A, The expression of Hox genes differentiates the Pre-EMT vagal/trunk neural crest cell from the Pre-EMT cranial neural crest cells. were detected in mature neural tube organoid. The migratory neural crest cells that were spotted migrating out from the organoid are cranial neural crest cells as they are lack of Hox gene expression. **B**, Plotting of the markers of each step: Pre-EMT neural crest (*Bmp6*$^{+}$ *Gdf7*$^{+}$), Delamination (*Dlx5*$^{+}$, *Pdgfra*$^{+}$), and Migratory neural crest cells (*Sox10*$^{+}$, *Foxd3*$^{+}$) captured the

emergence, delamination, and migration of neural crest cells derived from neural tube organoid. The RNA velocity streamlines support this transcriptomic event from preEMT state to delamination and migration. All the plots were generated from the same data set analysis of Fig. 4.

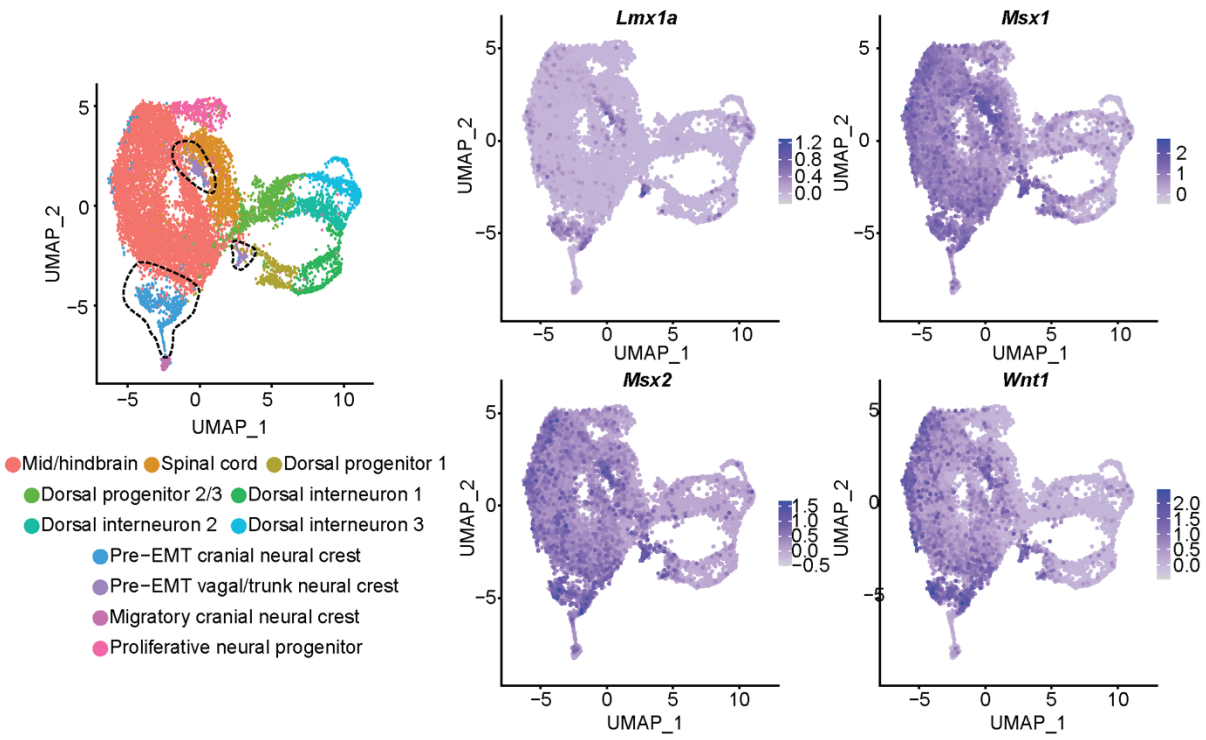

Fig. S12. Neural crest cells emerge from the roof plate-fate cells in the neural tube organoid. Roof plate markers, *Lmx1a*, *Msx1*, *Msx2*, and *Wnt1*, were distinctively expressed in the Pre-EMT neural crest clusters (both cranial and vagal/ trunk neural crest, in dotted circles). This result indicates that the neural crest cells emerge from the roof plate-fate cells in neural tube organoids which aligns with the neural crest development *in vivo* where the neural crest cells emerge from the roof plate of the neural tube. All the plots were generated from the same data set analysis of Fig. 4.

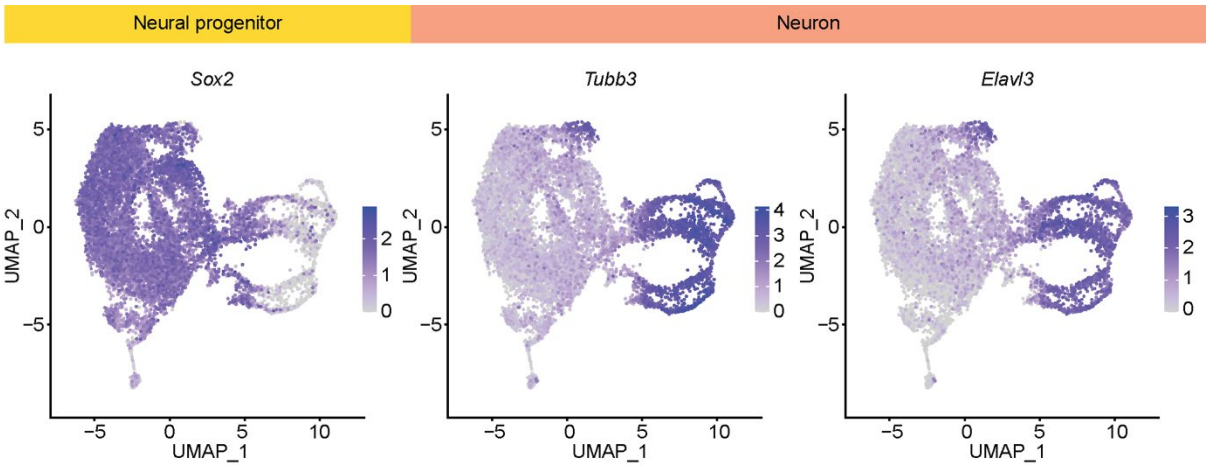

Fig. S13. scRNAseq captured the transcriptomic event of neural differentiation from neuroprogenitor to neurons. The cells from D6-D7 organoids were mostly neural progenitor expressing *Sox2* and then were differentiated into more mature neurons expressing *Tubb3* and *Elavl3* by D10. All the plots were generated from the same data set analysis of Fig. 4.

Movie 1. Self-elongation of the neural tube organoid. The organoids were stained with live cell actin probe to visualize the lumen and the actin in general of the organoids. **Part 1**, Time-lapse imaging from D0 to D6 showing the self-elongating neural tube organoid formation from a single cell with 10X air objective on Nikon Eclipse Ti inverted microscope. **Part 2**, Time-lapse imaging between D4 and D6 with 1 hour of interval with 10X air objective on Nikon Eclipse Ti Inverted Microscope. **Part 3**, Time-lapse imaging between D5 and D6 with 5 min of interval with 60X oil objective on Visitron CSU-W1. Those time-lapses revealed that the neural tube organoid self-elongate and its lumen elongate simultaneously keeping the neural canal-like structure.

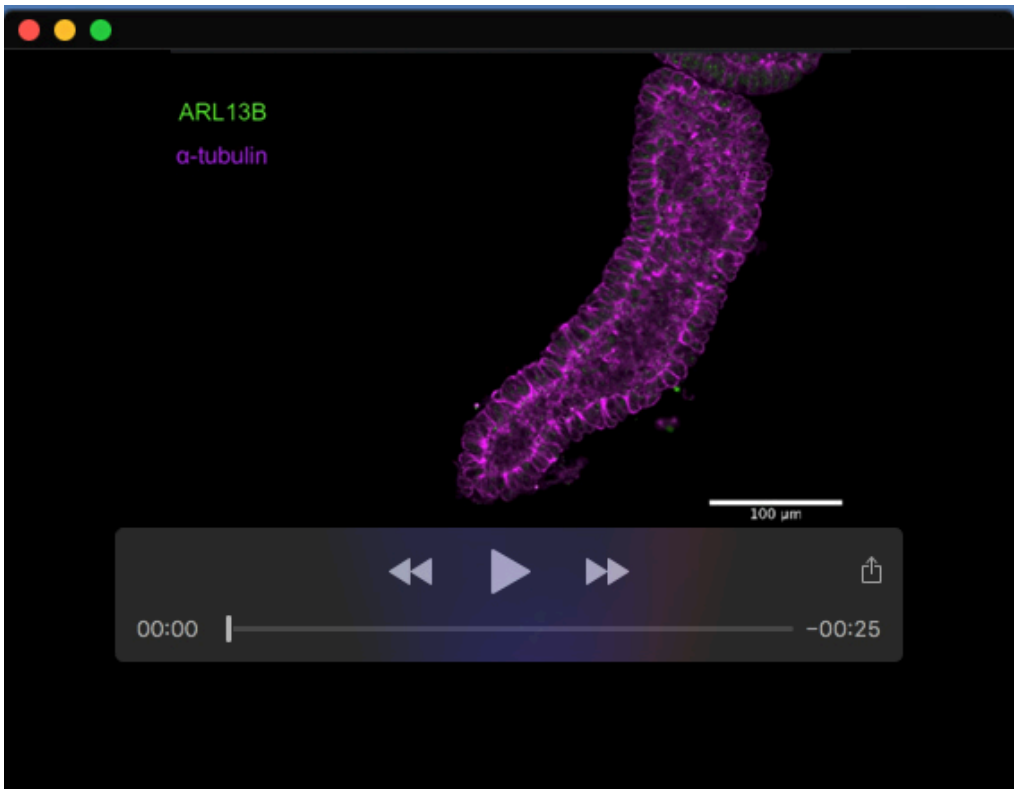

Movie 2. Primary cilia in the neural tube organoid. The organoids from D6 were immunostained against ARL13B (primary cilia) and acetylated α-tubulin and the confocal images were taken by Zeiss LSM 700 Inverted Microscope with 20X air or 63X oil objective. This result shows the primary cilia expressing ARL13B are localised at the apical membrane of the neural tube organoid which resembles the neural tube *in vivo*.

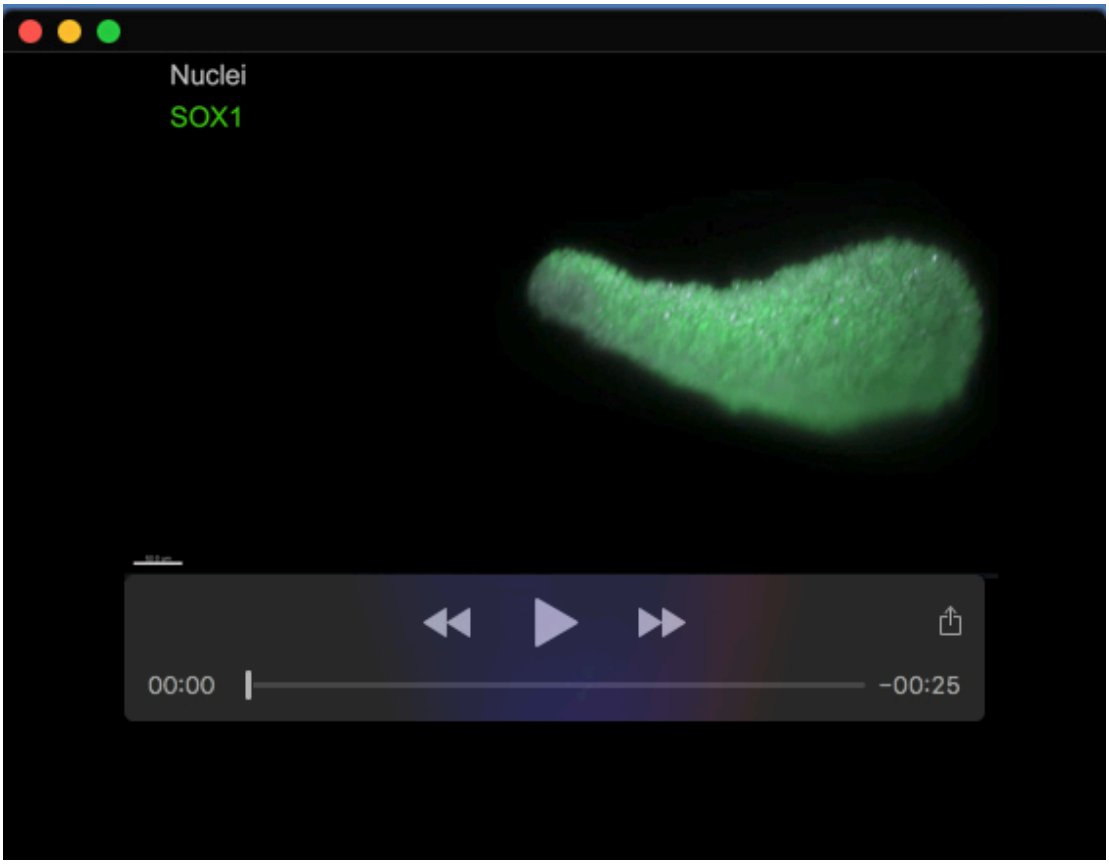

Movie 3. Neural canal-like structure in neural tube organoid. The organoids from D6 were stained against SOX1 (neuroectoderm), Ki67 (proliferating cell), and actin and the images were taken by Zeiss Lightsheet Z1 with 20X water objective. 3D projection of the images (IMARIS, Bitplane) clearly shows the actual tubular structure of the organoid with the hollow and elongated lumen in the middle of the neural tube organoid that recapitulates the neural canal *in vivo*. Scale bar is 50 μm.

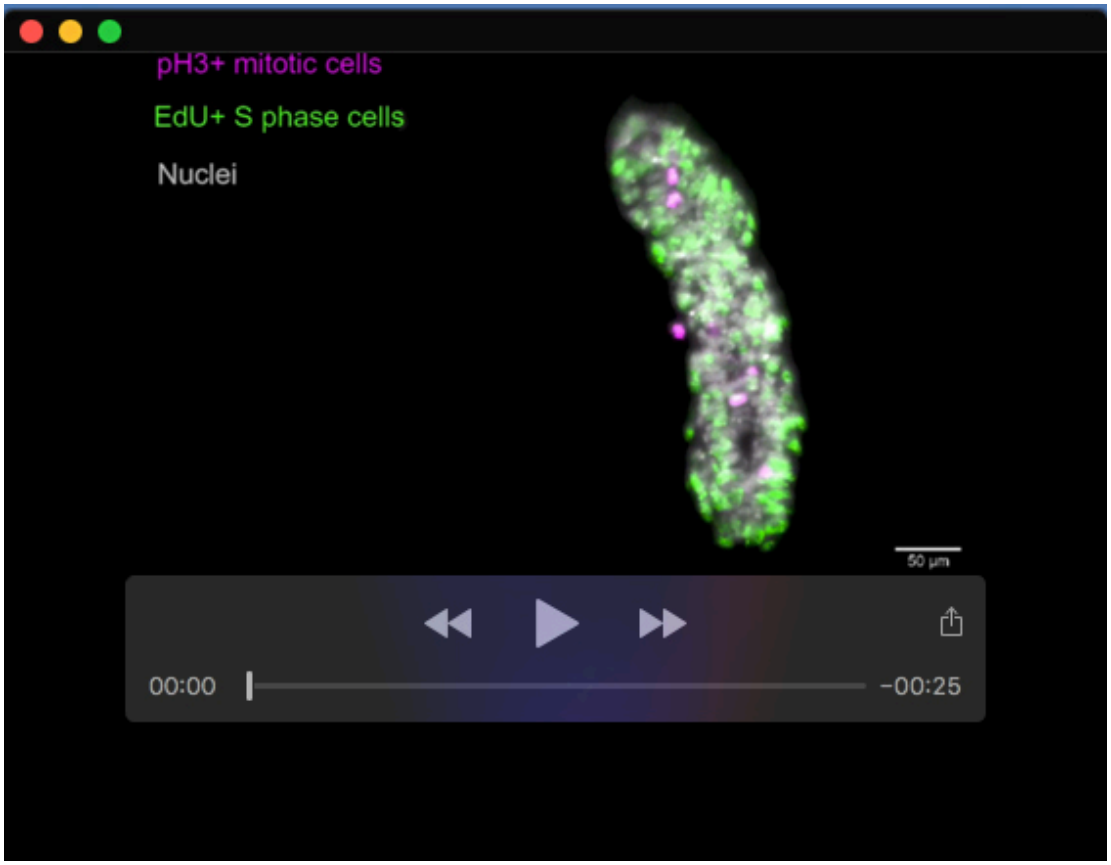

Movie 4. Interkinetic nuclear migration in the neural tube organoid. Part 1, The organoids from D6 were stained against $pH3^+$ mitotic cells (magenta) and S phase cells (green) and the images were taken by Zeiss Lightsheet Z1 with 20X clearing objective. In both horizontal axis and longitudinal axis, $pH3^+$ mitotic cells were observed at the apical domain and EdU^+ S phase cells were observed at the basal domain of the neural tube organoid. This result implies the interkinetic nuclear migration of the cells in the neural tube organoid. **Part 2**, Time-lapse imaging of the neural tube organoid stained by live cell actin probe with 5 min of interval between D5 and D6 obtained by Visitron CSU-W1 with 60X oil objective. This time-lapse captured the interkinetic nuclear migration of the cells in the neural tube organoid: the cells go to apical domain of the organoid, divide, and reconstitute the epithelium, as the developing neuroepithelial cells do *in vivo*.

Movie 5. Maturation of the neural tube organoid. Time-lapse imaging of the neural tube organoids (re-embedded in Matrigel on D6) from D6 to D8 with 1 hour of interval taken by Nikon Eclipse Ti Inverted Microscope with 20X air objective. **Part 1**, the neural crest cells emerge and migrate out from the neural tube organoid. **Part 2**, the neurite extends from the neural tube organoid meaning the emergence of mature neurons.

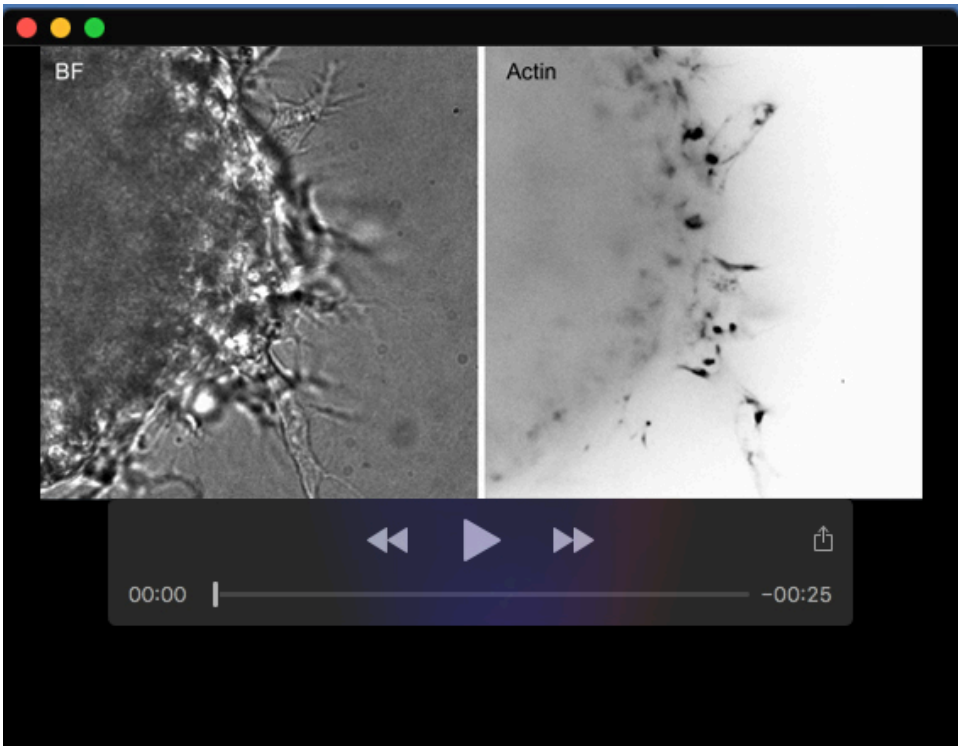

Movie 6. Neural crest cells: delamination, cell division, and phagocytosis. Time-lapse imaging of the mature neural tube organoid from D6 to D8 with 5 min of interval by Visitron CSU-W1 with 60x oil objective captured the delamination, cell division, and phagocytosis of neural crest cells derived from neural tube organoid.

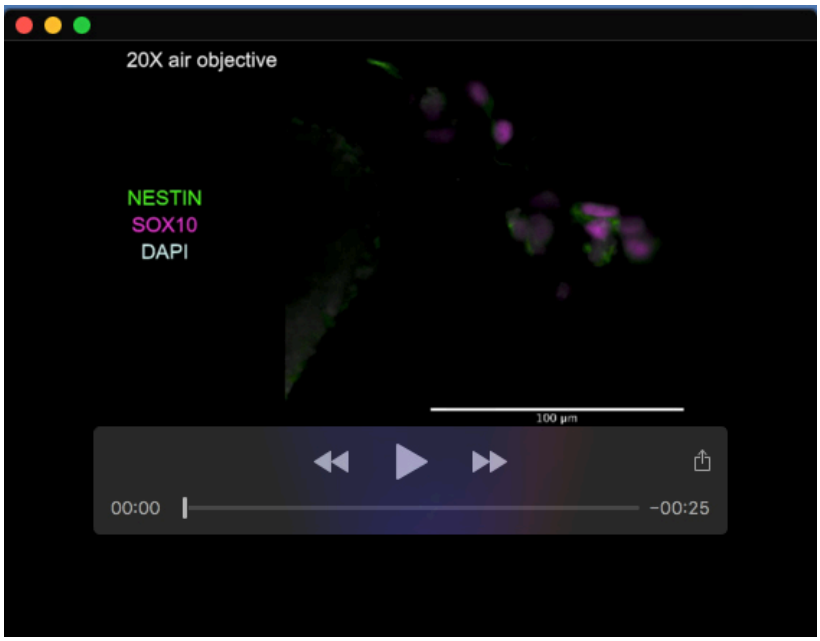

Movie 7. 3D migration of the neural crest cells. Confocal imaging of the neural tube organoids (re-embedded in Matrigel on D6 and cultured until D8) with z-stack shows the neural crest cells migrate out from the organoid three-dimensionally. The images were taken by Zeiss LSM700 inversed with 20X air objective and 40X oil objective. The migrating cells outwards from the organoid expressed neural crest cell markers, namely, NESTIN and SOX10. The 3D view of the Z-stack confocal images was processed on IMARIS (Bitplane).

Table S1. Embedding cell densities: self-elongating neural tube organoids require the optimal embedding cell numbers of each mESC line

Cell Line	Cells/10µL Matrigel drop
Sox1^{eGFP};*Bra*^{mCherry} double reporter (SBr)	1125
Wild-type of SBr	1125
Sox1^{GFP} reporter	1000
Sox10^{GFP} reporter	1000

Table S2. Primer sequences used for quantitative PCR

Probe	Primer Forward	Primer Reverse
Oct4	TGG AGG AAG CCG ACA ACA ATG AGA	TGG TGC CTC AGT TTG AAT GCA TGG
Fgf5	TCT CCT TTT ATC TGC CCC CT	GAG CAG ATG CAC TCA TTC CA
Otx2	GCA GAG GTC CTA TCC CAT GA	CTG GGT GGA AAG AGA AGC TG
Sox2	CAT GAG AGC AAG TAC TGG CAA G	CCA ACG ATA TCA ACC TGC ATG G
Sox1	AGA CAG CGT GCC TTT GAT TT	TGG GAT AAG ACC TGG GTG AG
Pax6	CTA CCA GCC AAT CCC ACA GC	TTC GGC CCA ACA TGG AAC
Hoxa2	CTC GGC CAC AAA GAA TCC CT	GGG GTC TGC AAA GGT ACT TG
Hoxb4	CAC GGT AAA CCC CAA TTA CGC	CGC GTC AGG TAG CGA TTG
Hoxc4	AGC ACG GTG AAC CCC AAT TA	GGC GAT CTC GAT CCT TCT CC
Hoxc5	ATG AGC CAC GAG ACG GAT G	GCG AGT GAG GTA GCG GTT AAA
Hoxc6	ACA CAC AGA CCT CAA TCG CT	ACC CCA CTG TGC GAA TTC AT
Hoxc8	GAT GAG ACC CCA CGC TCC T	CTT CAA TCC GGC GCT TTC TG
Hoxc9	GGA CCC TAG CAA CCC CGT	CGA CGG TCC CTG GTT AAA TAC A
Hoxc10	GTT TTG GGG TGT TGT GTG TG	TTG CAT GGA GAA CAG AAT GC
Hoxc11	CCG TCT CTT CCT TCC TAC CC	CGA GTA GCT GTT CCG ATG GT
Hoxc12	GCG AGT TTC TGG TCA ACG A	TTT TCA TTC TCC GGT TCT GG
Hoxc13	TCC CTG TTG AAG GCT ACC AG	CTC ACT TCG GGC TGT AGA GG
Lmx1a	CCC TTG TCT GGA CTC TAC CC	CGG TTG AGT CTA GCT TCC CG
Pax3	TGC CCA CAT CTC AGC CCT AT	AAT GAA AGG CAC TTT GTC CAT ACT
Pax7	CGA CTC CGG ATG TGG AGA AAA	TCT GAG CAC TCG GCT AAT CG
Dbx1	AAG CCC TGG AGA AGA CGT TC	CGC CAT TTC ATG CGT CGA TT
Dbx2	CCG AAG GAT GAA ATG GCG GA	TGG CTG GGA GAC TTC CCA TA
Nkx6-2	AGT ATT TGG CAG GCC CAG AG	GCT TCT TTT TAG CCG ACG CC
Olig2	TTA CAG ACC GAG CCA ACA CC	TGG CCC CAG GGA TGA TCT AA
Nkx2-2	GGT TCC AGA ACC ATC GCT ACA	TCC ACC TTG CGG ACA CTA TG
Foxa2	TTT AAA CCG CCA TGC ACT CG	CTC ACG GAA GAG TAG CCC TC
Shh	ATG TGT TCC GTT ACC AGC GA	ATA TAA CCT TGC CTG CCG CT
Gapdh	GCA CAG TCA AGG CCG AGA AT	GTG GTT CAC ACC CAT CAC AA

Table S3. Primary antibodies used in immunostaining

Target	Species	Dilution	Cat. No.	Supplier
OCT3/4	mouse	1:200	SC-5279	Santa Cruz Biotechnology
SOX1	goat	1:20	AF3369	R&D Systems
PAX6	rabbit	1:200	901301	BioLegend
CD133/Prominin-1	rat	1:200	14-1331-82	Invitrogen
SOX2	rabbit	1:1000	ab97959	abcam
T/Brachyury	goat	1:500	AF2085	R&D Systems
Phospho-Histone H3 (Ser10)	rabbit	1:500	06-570	Merck
ARL13B	rabbit	1:200	17711-1-AP	Proteintech
Acetylated alpha tubulin (Lys40)	mouse	1:200	6-11B-1	Thermo Fischer
NGFR (p75)	mouse	1:200	sc-271708	Santa Cruz Biotechnology
BRN3a	rabbit	1:500	AB5945	Merck
AP2α	mouse	1:50	sc-12726	Santa Cruz Biotechnology
NESTIN	mouse	1:100	ab11306	abcam
SOX10 [SP267]	rabbit	1:25	ab227680	abcam
TUJ1	mouse	1:500	MMS-435P	Covance
GFAP	rabbit	1:500	Z0334	DAKO
S100β (EP1576Y)	Rabbit	1:100	ab52642	abcam
SM22a	rabbit	1:200	ab14106	abcam
ZO-1	rat	1:8	R26.4C	DSHB
PKCζ	mouse	1:200	sc-17781	Santa Cruz Biotechnology
KI67 (Sp6)	rabbit	1:200	MA5-14520	Invitrogen
FOXA2	rabbit	1:250	ab108422	abcam
OLIG2	rabbit	1:500	AB9610	Millipore
Peripherin	rabbit	1:150	AB1530	Millipore

Table S4. Secondary antibodies used in immunostaining

	Dilution	Cat. No	Supplier
Donkey anti-goat Alexa Fluor 647	1:500	705-606-147	Jackson ImmunoResearch
Donkey anti-goat Alexa Fluor 488		A-11055	ThermoFisher Scientific
Donkey anti-mouse Alexa Fluor 568		A-10037	
Donkey anti-rabbit Alexa Fluor 647		A-31573	
Goat anti-rat Alexa Fluor 647		A-21247	
Donkey anti-rabbit Alexa Fluor 568		A-10042	
Donkey anti-mouse Alexa Fluor 647		A-31571	

Table S5. Dyes used in staining: S-phase cell detection, nuclear staining, actin staining, and live cell actin imaging.

	Dilution	Cat. No	Supplier	Purpose
Click-iT™ EdU Cell Proliferation Kit for Imaging, Alexa Fluor™ 647 dye	N/A	C10340	Invitrogen	S-phase cell detection
DAPI	1:500	D1306	Invitrogen	Nuclear dye
Alexa Fluor™ 647 Phalloidin	1:500	A22287	Invitrogen	Actin dye
sir-actin	1:1000	SC001	Spirochrome	Live cell actin dye
BODIPY™ 493/503	1:1000	D3922	ThermoFisher Scientific	Lipid droplet

Table S6. Probe sequences used for whole-mount single-molecule fluorescence *in situ* hybridisation (smFISH) (Excel file)

Click here to download Table S6

Table S7. Marker list for cell type of D6 organoids on Figure 2 (Excel file)

Click here to download Table S7

Table S8. Marker list for cell type of D6-D10 organoids on Figure 4 (Excel file) For cell type identification, we have referenced mainly two single cell transcriptomic analysis reports on developing mouse neural tube: spatial and temporal dynamics of gene expression in spinal cord (Delile *et al.*, 2019) and neural crest development (Soldatov *et al.*, 2019).

Click here to download Table S8